

Distinct stellar populations in the inner bars of double-barred galaxies

A. de Lorenzo-Cáceres^{1,2*}, J. Falcón-Barroso^{1,2†}, and A. Vazdekis^{1,2‡}

¹*Depto. Astrofísica, Universidad de La Laguna (ULL), E-38206 La Laguna, Tenerife, Spain*

²*Instituto de Astrofísica de Canarias (IAC), E-38205 La Laguna, Tenerife, Spain*

Accepted xxx. Received xxx; in original form xxx

ABSTRACT

Numerical simulations of double-barred galaxies predict the build-up of different structural components (e.g., bulges, inner discs) in the central regions of disc galaxies. In those simulations, inner bars have a prominent role in the internal secular evolution of their host galaxies. The development of bulges and inner discs is, however, poorly understood observationally due to the small number of studies focusing on the stellar populations of these systems. In order to provide constraints on the relevant processes inducing the creation of these components in the presence of inner bars, we have carried out a detailed kinematical and stellar population analysis in a sample of four double-barred galaxies, ranging from SB0 to SBb, observed with integral-field spectroscopy. We find that the inner bars present distinct stellar population properties, being younger and more metal-rich than the surrounding bulges and outer bars. While we detect signatures of gas inflow through the inner bars, we find no evidence of associated star-forming regions or newly-formed structures around them. This result suggests that, regardless of their formation scenario, *at present* these inner bars are playing a moderate or even a minor role in the morphological evolution of this sample of double-barred galaxies.

Key words: galaxies: kinematics and dynamics — galaxies: evolution — galaxies: individual: NGC 2859 — galaxies: individual: NGC 3941 — galaxies: individual: NGC 4725 — galaxies: individual: NGC 5850

1 INTRODUCTION

Bars have been traditionally considered key drivers of the internal secular evolution of disc galaxies. In fact, bars are non-axisymmetric structures that can redistribute the angular momentum of a galaxy, thus favouring the transport of gas through them to the inner regions where it may trigger star formation (e.g., Muñoz-Tuñón et al. 2004; Sheth et al. 2005). This internal, slow process competes with fast external drivers, such as mergers or interactions, as the main scenarios responsible for the formation of new spheroidal components and bulges at the galaxy centres (see Kormendy & Kennicutt 2004, for a review). Moreover, bar-driven structural evolution of disc galaxies can produce significant kinematical and morphological changes, such as the increase of the bulge-to-disc ratio, which in turn could lead to a parallel evolution along the Hubble sequence (Pfenniger & Norman 1990; Friedli & Martinet 1993).

The bar-driven evolution scenario is backed by the large fraction of barred galaxies found in the nearby Universe (e.g., Eskridge et al. 2000; Marinova & Jogee 2007; Aguerri et al. 2009) to $z \sim 1$

(e.g., Elmegreen et al. 2004; Jogee et al. 2004, but see also Sheth et al. 2008; Cameron et al. 2010). Among local early-type barred spirals, $\sim 30\%$ have been found to host an inner, secondary bar embedded in the main, larger bar (e.g., Erwin & Sparke 2002; Laine et al. 2002; Erwin 2004), and a two-bar system has been observed even at $z \sim 0.15$ by Lisker et al. (2006). Therefore, double-barred galaxies are also rather common systems and, in the same way as a single bar, they may contribute to the gas inflow towards the central regions. Moreover, the material driven inwards by a nested-bar system may reach the innermost parts and feed the active galactic nuclei (Shlosman et al. 1989, 1990, but see also Ho et al. 1997; Márquez et al. 2000). It is hence clear that inner bars may be playing an important role in the shaping and evolution of spiral galaxies.

The formation of inner bars and their efficiency in driving the gas inflow have been extensively studied by numerical simulations. These works usually require the presence of a dissipative component to form a stable double-barred system, so the main bar is formed first, and the gas flows along it and is finally trapped by the x_2 orbits. The x_2 family is composed by elliptical orbits which are elongated in the direction perpendicular to the main bar major axis (Contopoulos & Papayannopoulos 1980). The gas trapped by the x_2 orbits then forms the inner bar (Friedli & Martinet 1993; Heller et al. 2001; Rautiainen et al. 2002; Shlosman & Heller 2002; Englmaier & Shlosman 2004). Only Debattista & Shen (2007)

* adler@iac.es

† jfalcon@iac.es

‡ vazdekis@iac.es

are able to create a purely stellar inner bar from collisionless N -body simulations, but with the peculiar initial requirement of having a rapidly rotating component at the centre. Except for this particular case, most numerical simulations produce gas-rich bars capable of transporting material to the central regions (e.g., Heller et al. 2007), thus contributing significantly to the secular evolution of their host galaxies (Pfenniger & Norman 1990).

In an effort to constrain the role of bar-related secular processes in shaping the central regions of galaxies, several authors have compared the properties of bulges in barred and non-barred galaxies. Moorthy & Holtzman (2006) analysed a sample of face-on spirals and obtained a trend toward younger ages for the bulges of barred galaxies; on the contrary, Jablonka et al. (2007) found no differences between the stellar population properties of edge-on barred and non-barred galaxies. Pérez & Sánchez-Blázquez (2011) studied the bulge properties of a sample of early-type galaxies hosting bars, and found significant differences with respect to their unbarred counterparts, the former being more metal-rich and slightly more α -enhanced. The metallicity of the bulge was very similar to that of the bar, and Pérez & Sánchez-Blázquez (2011) concluded that both structures form simultaneously but with different episodes of star formation. Finally, Coelho & Gadotti (2011) compared the age and metallicity values for a sample of bulges hosted by barred and non-barred galaxies; their results suggested that bars do affect the mean stellar age of bulges, in such a way that bars actually triggered star formation at the centres of their galaxies.

None of the previous studies includes specific data for double-barred galaxies. In fact, there is a notable lack of kinematical and stellar population analyses of these kinds of objects in the literature, mainly due to the strict observational conditions needed to take spectra of these structurally complex objects, which are composed of two bars randomly oriented (e.g., Friedli & Martinet 1993), very different in size (Erwin & Sparke 2002), and independently rotating (e.g., Shlosman & Heller 2002; Corsini et al. 2003). Pérez et al. (2007), Pérez et al. (2009), and Sánchez-Blázquez et al. (2011) studied the stellar populations of a sample of barred galaxies including some double-bars; they found positive, null, and negative metallicity gradients along the bars, independently of their age profiles, and also concluded that bulges of barred galaxies tend to be more metal-rich than those belonging to unbarred galaxies of similar velocity dispersions. However, these authors focussed on the main bars and did not pay special attention to the behaviour of inner bars. Only de Lorenzo-Cáceres et al. (2012) studied in detail the stellar population properties of the bulge, inner bar, and outer bar of a double-barred galaxy: NGC 357. They found that the three structures are nearly coeval, with an age around 8 Gyr; the bulge and inner bar also show the same metallicity and α -enhancement values, but the outer bar is clearly less metal-rich and more [Mg/Fe] overabundant than the inner regions. The interpretation of these results was that the inner bar and bulge were effected by the redistribution of existing stars.

The analysis performed by de Lorenzo-Cáceres et al. (2012) relied on long-slit spectroscopy along both bars, so their results could not address the regions outside the bars that might be quite important given the structural complexity of double-barred galaxies. Integral-field spectroscopy seems to be the most suitable option for studying these kinds of objects, as shown by Moiseev (2001), Moiseev et al. (2004), and de Lorenzo-Cáceres et al. (2008). These three works are focused on the kinematics of double-barred galaxies, previously studied through long-slit spectroscopy by Emsellem et al. (2001), and they highlight the importance of including the spatial information outside the major axes of the bars in the analysis.

In particular, de Lorenzo-Cáceres et al. (2008) presented the discovery of the σ -hollows, two local decreases of the velocity dispersion values exactly at the edges of the inner bars. With the aid of numerical simulations, the authors infer that these hollows are due to the contrast between the different velocity dispersion values of the bulge and the inner bar, and they represent the only known kinematical signature of the presence of a stellar inner bar. It is important to notice that although the σ -hollows have also been observed in long-slit spectra (de Lorenzo-Cáceres et al. 2012), their discovery is closely linked to the integral-field nature of the work performed by de Lorenzo-Cáceres et al. (2008).

We present here a detailed kinematical and stellar population analysis of the sample of double-barred galaxies, already introduced in de Lorenzo-Cáceres et al. (2008), studied through integral-field spectroscopy. For the first time, we analyse the spatial distribution of the age, metallicity, abundance ratio, and other relevant properties of double-barred galaxies in order to constrain their formation scenarios and role in secular evolution. The paper is organised as follows: in Section 2 we describe the sample selection and observations, whereas the data reduction is summarized in Section 3. In Section 4 we perform a photometric analysis to check the parameters of the inner and outer bars. Extensive descriptions of the kinematical and stellar population analyses, and the direct results obtained from them, can be found in Sections 5 and 6, respectively. The implications of these results for the formation scenarios of double-barred galaxies and the role of inner bars in the galaxy evolution are discussed in Section 7. Finally, a summary of the work and the main conclusions are compiled in Section 8.

2 SAMPLE SELECTION, OBSERVATIONS AND INSTRUMENTAL SETUP

The sample is composed of four double-barred galaxies: NGC 2859, NGC 3941, NGC 4725, and NGC 5850. These galaxies were selected from the catalogue of Erwin (2004), paying special attention to the length and size of the inner bars. The main requirement for building the sample was that the inner bars were big enough to be well mapped within the SAURON field-of-view (hereafter FoV), but they were also small enough to allow the mapping of the transition regions between the two bars. Note that the main bar is usually larger than the total FoV.

The inclinations of the four galaxies range between 25° and 50° ; these intermediate values allow us to recover the line-of-sight kinematics, with only a moderate mixing of the components due to projection. Since the main goal is to perform the stellar population analysis, only early-type galaxies were considered in order to avoid additional handicaps, such as complex spiral structures. In particular, the galaxies were selected to have almost no dust, although it is worth noting here that our stellar population analysis is based on the measurement of the line indices which are little affected by dust (see MacArthur 2005). Finally, NGC 3941 and NGC 4725 are classified as Seyfert 2 galaxies (Véron-Cetty & Véron 2006), whereas NGC 2859 presents no signs of nuclear activity and NGC 5850 is considered a LINER (Low Ionisation Nuclear Emission Region, see Section 5.2.2 for further details on the LINER classification of this galaxy; Bremer et al. 2012). The bar lengths, ellipticities, position angles (hereafter PA), and other relevant properties for the sample galaxies are summarized in Table 1.

The four double-barred galaxies have neutral atomic gas, as shown in the HI studies by Serra et al. (2012) for NGC 2859 and NGC 3941, Wevers et al. (1984) for NGC 4725, and Higdon et al.

Table 1. Main properties of the double-barred sample.

Name (1)	RC3 Type (2)	D (3)	i (4)	Position angle (5)			Semi-major axis (6)		ϵ_{max} (7)	
				Disc	Inner bar	Outer bar	Inner bar	Outer bar	Inner bar	Outer bar
NGC 2859	(R)SB(r)0 ⁺	25.4 Mpc	25°	90°	62°	162°	4.1 arcsec	34 arcsec	0.31	0.40
NGC 3941	SB(s)0 ⁰	18.9 Mpc	51°	10°	30°	166°	3.2 arcsec	21 arcsec	0.21	0.47
NGC 4725	SAB(r)ab	12.4 Mpc	42°	40°	141°	50°	5.6 arcsec	118 arcsec	0.20	0.67
NGC 5850	SB(r)b	28.5 Mpc	30°	163°	50°	116°	5.9 arcsec	63 arcsec	0.30	0.68

(1) Galaxy name; (2) Morphological type from de Vaucouleurs et al. (1991); (3) distance to the galaxy, from Tully (1988). Throughout the whole paper we assume $H_0=75 \text{ km s}^{-1} \text{ Mpc}^{-1}$; (4) galaxy inclination; (5) position angle of the major axis (disc) and the two bars; (6) bar lengths, estimated as the semi-major axes of maximum isophotal ellipticity; (7) maximum isophotal ellipticity of the bars ($\epsilon = 1 - b/a$). Columns (4), (5), (6), and (7) are taken from Erwin (2004) (except for the PA of the inner bar of NGC 3941, which is taken from Erwin & Sparke 2003). NOTE: there is an erratum in Erwin (2004) so that the position angle of the inner bar of NGC 3941 is given as 85°, which is not correct. Erwin & Sparke (2003) provide a value between 20° and 35°; taking into account the alignment of the σ -hollows (see Section 5.1.1), we finally assume a position angle of 30° for NGC 3941, in agreement with the measurements of Erwin & Sparke (2003).

Table 2. Summary of the observations.

Name (1)	Integration time (2)	Seeing (3)	Central S/N (4)
NGC 2859	4 hours	0.9 arcsec	353
NGC 3941	3.5 hours	0.6 arcsec	389
NGC 4725	3 hours	1 arcsec	252
NGC 5850	4 hours	1.3 arcsec	161

(1) Galaxy name; (2) total integration time for each galaxy; (3) mean integration time-weighted seeing value during the observation of the galaxy; (4) maximum S/N value reached for each galaxy. This S/N corresponds to a spectrum in the central region of the galaxy, where the surface brightness profile presents also a maximum.

(1998) for NGC 5850. The HI is mainly located in external ring structures, whereas there is no neutral atomic gas in the central regions we are interested in. Regarding the neutral molecular gas, CO observations have been taken for NGC 2859 (Bieging & Biermann 1977; Wardle & Knapp 1986; Petitpas & Wilson 2004), NGC 3941 (Bontempi et al. 2012), and NGC 4725 (Sheth et al. 2005). If detected at all, the molecular gas fractions were very low. Particularly interesting is the case of NGC 5850, for which a very large amount of molecular gas is found in the central region, possibly driven there through the main bar (Petitpas & Wilson 2004). Moreover, high resolution interferometric maps of NGC 5850 obtained by Leon et al. (2000) reveal that most of this central molecular gas is concentrated in a single peak, which is slightly off-centred towards the North.

Our new observations were carried out with the SAURON integral-field spectrograph, attached to the William Herschel Telescope (WHT) at the Observatorio del Roque de los Muchachos in La Palma, Spain. Data for the four galaxies were taken during four nights in 2007 April 14 and 16–18. Detailed information on the observations is found in Table 2. SAURON uses an array of lenslets to section the FoV into 1431 *spaxels* (spatial elements). The spectrograph was operated in the Low-Resolution (LR) mode, which provides a $33 \times 41 \text{ arcsec}^2$ FoV with a spatial scale of $0.94 \text{ arcsec spaxel}^{-1}$. The grating, which has $514 \text{ lines mm}^{-1}$, covers the wavelength range between 4800 and 5380 Å. These characteristics imply a sampling of 1.1 Å pixel^{-1} and a spectral resolution of 3.74 Å (FWHM), which corresponds to $\sigma_{\text{inst}} \sim 94 \text{ km s}^{-1}$. The detector is an EEV12 CCD composed of 2148×4200 pixels of $13.5 \times 13.5 \mu\text{m}^2$ each.

The observations were taken with the galaxies centred on the FoV of the lenslet array. The instrument was orientated so that the major axis of the FoV is parallel to the major axis of each galaxy disc. The true orientation of our maps on the sky is indicated in Appendix A. The total integration time for the galaxies ranges between three and four hours, in exposures of 30 minutes each. The dithering of 1 arcsec applied between the different exposures allows a correction of possible bad pixels of the CCD. Apart from the object lenslets, SAURON has an additional array of 146 lenses for simultaneous sky observations. These spectra are taken at a distance of 1.9 arcmin from the main FoV. The instrumental scheme and setup possibilities of SAURON are described in Bacon et al. (2001).

At least one Neon lamp exposure was obtained before and after each galaxy exposure, in order to check the focus of the instrument and to assure an accurate wavelength calibration. Sky flat fields were taken during the twilights, whereas Tungsten lamp flat fields and several Lick standard stars of different spectral types were observed throughout each night. The seeing value ranged from 0.5 to 1.6 arcsec.

3 DATA REDUCTION

The data reduction was performed using the specifically designed XSAURON package, following the prescriptions given in Bacon et al. (2001) and in Emsellem et al. (2004). The first steps are the bias subtraction and the extraction of the spectra. For the latter, it is necessary to create a mask which indicates which pixels of the CCD correspond to the same spectrum. Such a mask is characteristic of each observation run. Once the individual spectra are extracted, they are wavelength-calibrated, flat-field corrected, and cleaned from cosmic rays. Data for each galaxy are then homogenised by degrading all the spectra to the same resolution. Then, the spectra are flux-calibrated using the observed spectrophotometric standard stars. Finally, we align and sum up the spectra from different exposures, and we create the cubes in the Euro3D format (Kissler-Patig et al. 2004).

In order to assure the minimum signal-to-noise ratio (hereafter S/N) required for our analysis, we spatially bin the final datacubes using the Voronoi 2D binning algorithm of Cappellari & Copin (2003). Thus, we create compact bins with a minimum S/N of ~ 60 per spectral resolution element, which allows us to measure the higher order moments of the line-of-sight velocity distribution

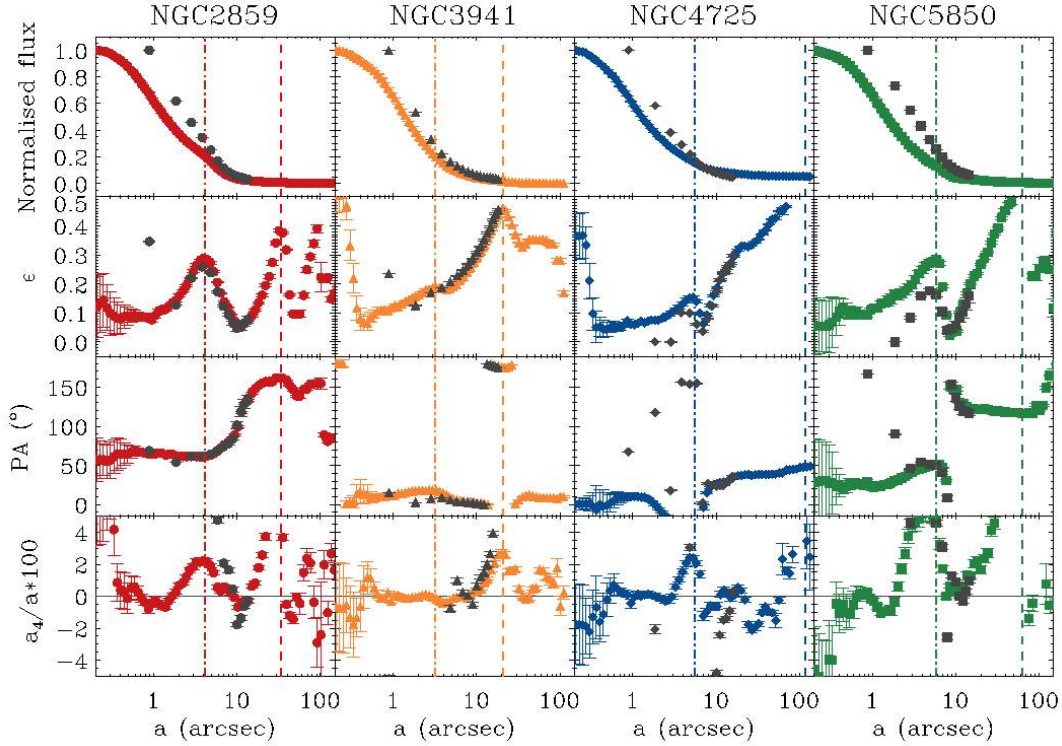


Figure 1. From top to bottom: normalised flux, ellipticity, PA, and the fourth cosine Fourier coefficient (a_4) profiles resulting from fitting ellipses to the isophotes of *i*-band images from SDSS (coloured symbols) and to the reconstructed SAURON flux maps (overplotted grey symbols) for the four double-barred galaxies: NGC 2859, NGC 3941, NGC 4725, and NGC 5850. The x-axes represent the semi-major lengths of the fitted ellipses. The dot-dashed and dashed vertical lines indicate the inner and outer bar lengths for each galaxy, as given by Erwin (2004).

(hereafter LOSVD), h_3 and h_4 . Note, however, that the spectra corresponding to the central regions of the galaxies have already S/N values well above 60 \AA^{-1} , so they remain unbinned.

4 PHOTOMETRIC ANALYSIS

The relevant bar parameters of the sample have been already analysed by several authors, mainly Erwin (2004) whose results are compiled in Table 1.

In order to assess whether we can *photometrically* resolve the different structures in our data, we have carried out ellipse fitting over the flux maps recovered after stacking our spectra in the wavelength direction. For this purpose we have made use of the KINEMTRY program (Krajinović et al. 2006), which calculates the best fitting ellipses in an analogous way to how it is done in the IRAF task ELLIPSE (Jedrzejewski 1987). The resulting normalised flux, PA, ellipticity, and the fourth cosine Fourier coefficient (a_4) profiles are shown in Figure 1, which confirms the inner and outer bar length estimates given by Erwin (2004, as indicated by the corresponding maxima in the ellipticity profiles). In the case of NGC 3941, the presence of the inner bar is difficult to appreciate in this photometric analysis due to its small size and ellipticity. Figure 1 also shows that the a_4 parameter tends to peak at the semi-major axis length of the two bars. This trend was already pointed out by de Lorenzo-Cáceres et al. (2012) for the case of the inner bar of the double-barred galaxy NGC 357. The four galaxies presented here are mainly shaped by discy isophotes ($a_4 > 0$) especially at the inner and outer bar ends,

with the exception of NGC 3941, for which the analysis in the inner bar region indicates pure ellipsoid isophotes.

The results obtained with the SAURON data are in good agreement with the profiles we measured using *i*-band images from the Sloan Digital Sky Survey (SDSS; York et al. 2000). This comparison is shown in Figure 1. Deviations occur only at the very central regions, due to PSF effects. This photometric analysis confirms that our data are well suited to the study of our sample of four double-barred galaxies.

5 STELLAR AND IONISED-GAS KINEMATICS

5.1 Stellar kinematics

To extract the stellar kinematics, we performed a full-spectrum fitting over the stellar spectra as described in Falcón-Barroso et al. (2006). The potential emission lines included in the SAURON spectral range (i.e., $H\beta$, [OIII]5007 and [NI]) were previously masked in order to work with the pure absorption contribution. We made use of the penalized pixel fitting (hereafter pPXF) routine developed by Cappellari & Emsellem (2004), which fits each stellar spectrum with a linear combination of a well-selected set of templates. In this case, we selected a subsample of the updated single stellar population models (SSPs) of Vazdekis et al. (2010, see also Falcón-Barroso et al. 2011), with evenly sampled ages and metallicities. A linear combination of those templates, adjusted to match the spectral resolution of our data, was convolved with a Gauss-Hermite function (Gerhard 1993; van der Marel & Franx 1993) to recover the best fitting four lowest-order moments of the LOSVD (velocity,

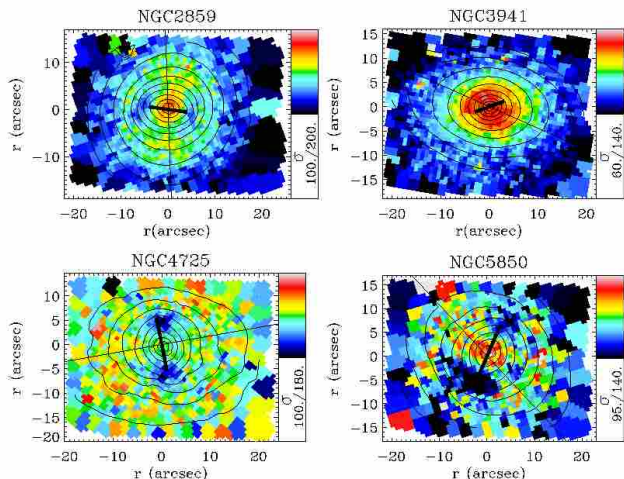


Figure 2. Stellar velocity dispersion maps, in km s^{-1} , for the four double-barred galaxies: NGC 2859, NGC 3941, NGC 4725, and NGC 5850. The length and position angle of the inner and outer bars are indicated by thick and thin lines, respectively. We have also overplotted the contours of the reconstructed total intensity maps. The σ -hollows are clearly seen at the edges of the four inner bars, as two spots with bluer colours (i.e., lower values) than the surroundings.

velocity dispersion, h_3 , and h_4). The resulting maps are presented in Appendix A. Although the galaxies show no dust content (see Section 2), the narrow wavelength coverage of SAURON additionally assures that our analysis is not affected by possible differential extinction.

5.1.1 The σ -hollows

The velocity and velocity dispersion maps for this sample of double-barred galaxies were already shown in de Lorenzo-Cáceres et al. (2008), where we presented the discovery of the σ -hollows. The σ -hollows are two symmetric, local decreases of the velocity dispersion values that appear exactly at the edges of the inner bars, with amplitudes with respect to their immediate surroundings ranging between 10 and 40 km s^{-1} , as seen in Figure 2. In de Lorenzo-Cáceres et al. (2008) we discussed different scenarios that might explain the presence of these hollows, concluding that they are just a matter of contrast between the σ values of the inner bar and the surrounding bulge.

The importance of the σ -hollows lies in that they are a signature of the inner bars. They are also clearly visible in the velocity dispersion profile of the double-barred galaxy NGC 357 (de Lorenzo-Cáceres et al. 2012), studied through long-slit spectroscopy with slits oriented along both the inner and outer bars. The amplitude of the hollows in NGC 357 is $\sim 20 \text{ km s}^{-1}$ and thus consistent with the values found in the present sample.

The σ -hollows have not been previously found in other works devoted to the study of the stellar kinematics of double-barred galaxies, probably due to the precise requirements needed for their detection. In fact, most existing observations of double-barred galaxies relied on long-slit spectroscopy along one direction, typically the major axis of the disc (e.g., Corsini et al. 2003). Only Emsellem et al. (2001) positioned the slit along the inner bar, but the S/N in their case was not high enough to clearly distinguish whether the hollows are present in their velocity dispersion profiles. Better suited integral-field spectroscopy was used by Moiseev et al. (2004)

with the MPFS instrument. However, their FoV ($16 \times 15 \text{ arcsec}^2$) prevented the detection of the σ -hollows signature in their sample.

It is interesting to note that none of the galaxies presented in this work shows a central σ -drop. The σ -drop is a local velocity dispersion minimum that appears at the centre of many spiral galaxies, usually related to a cold, newly-formed stellar component, such as an inner disc. Falcón-Barroso et al. (2006) find this signature in at least 46% of a sample of 24 early-type spirals, and other cases have been noticed in different samples (Márquez et al. 2003; Ganda et al. 2006; Comerón et al. 2008), especially in single-barred galaxies but also in double-barred galaxies (Emsellem et al. 2001). Given the high frequency of σ -drops in these kinds of objects, the fact that none of the four double-barred galaxies shown here presents this signature seems peculiar.

5.1.2 Kinematically decoupled inner discs

The stellar velocity maps of the four double-barred galaxies resemble those expected for unbarred galaxies: they do not seem to be affected by the presence of the inner nor the outer bars, and just show the rotation along the major axis of the main galaxy disc. However, for the three cases highlighted in Figure 3 (NGC 2859, NGC 4725, and NGC 5850), local velocity maxima and minima appear between 5 and 10 arcseconds of the galaxy centre, aligned also with the kinematical major axis. These decoupled structures are rotating faster than their surroundings and are probably indicating the presence of stellar inner discs. This hypothesis is supported by the h_3 maps also included in Figure 3, which show a clear anticorrelation with respect to the stellar velocities exactly at the locations of those features, as expected in the case of discs (Bureau & Athanassoula 2005). These features found in the velocity and h_3 maps are unlikely to be related to the inner bars given their completely different orientations.

5.2 Gas kinematics

Besides the stars, our galaxies show emission-line ionised gas, some of which fill in the absorption features in the observed spectra. A careful separation of this gas from the stars is crucial for a proper analysis of each tracer. Our four double-barred galaxies show significant amounts of gas, which we recovered by using the GANDALF code (Sarzi et al. 2006). This procedure allows us to recover the amplitudes and kinematics of the emission lines present in our wavelength range (e.g., $H\beta$, and the [OIII]4959,5007 and [NI]5198,5200 doublets). Our analysis shows that $H\beta$ and [OIII]5007 are the two most prominent lines. While we fitted both lines independently, i.e., they were not forced to have the same kinematics, the gas distribution and kinematics obtained for each line are very consistent for all galaxies except for NGC 5850, which is discussed in Section 5.2.2.

5.2.1 Possible evidence of gas inflow to the central region

The gas intensity maps for the four double-barred galaxies reveal interesting spiral structures, especially evident in the cases of NGC 2859 and NGC 3941. Moreover, the velocity maps also seem to be disturbed by these spirals, as their zero isovelocity curves appear twisted with respect to the kinematical minor axes. Figure 4 highlights the distortion of the velocity fields in comparison with the gas intensities. The spiral structures and the twisting of the velocity fields suggest there are gas streaming motions towards the

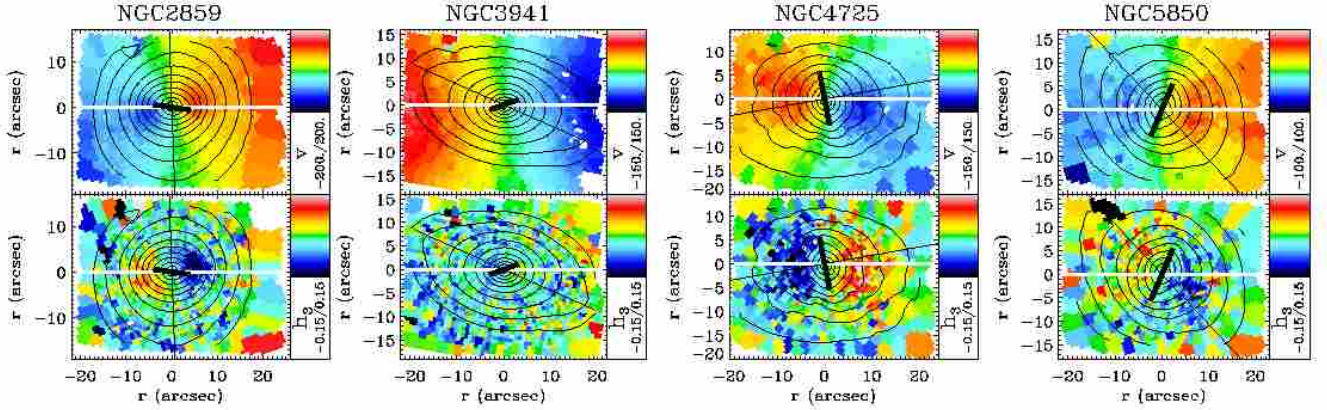


Figure 3. Stellar line-of-sight velocity (km s^{-1} ; top panels) and H_3 (bottom panels) maps for the double-barred sample. NGC 2859, NGC 4725, and NGC 5850 show evidence of a kinematically decoupled, corotating inner disc, seen as two local velocity maxima and minima in the velocity fields at a few arcseconds from the centres, with an anticorrelated counterpart at the same locations in the H_3 maps. We have overplotted the position angle and length of the inner (thick line) and outer (thin line) bars, and the contours of the reconstructed total intensity map, in order to highlight the fact that these decoupled inner discs are aligned with the semi-major axes of the galaxy discs (also indicated by a white line) and thus do not seem to be related to the inner bars.

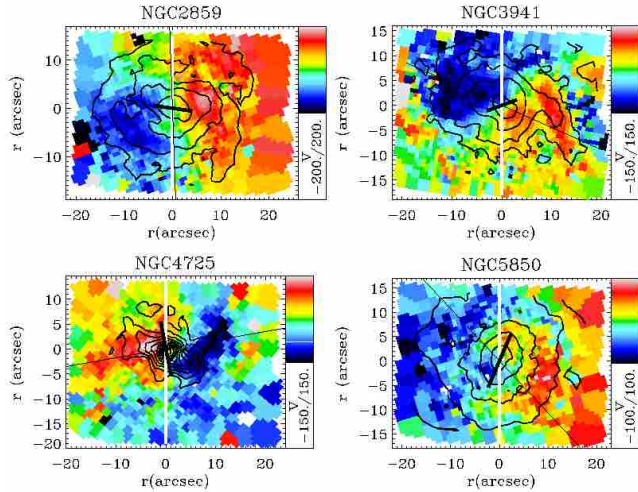


Figure 4. Gas velocity maps (km s^{-1}) corresponding to the $[\text{OIII}]\text{5007}$ emission line for the four double-barred galaxies. The zero isovelocity curves are clearly twisted with respect to the kinematical minor axes. The isodensity contours of the $[\text{OIII}]\text{5007}$ intensities are overplotted in order to emphasize the distortion of the velocity fields due to their spiral-like gas distributions. The black lines indicate the position and size of the inner (thick line) and outer (thin line) bars, whereas the white line shows the direction of the kinematical minor axes.

central region of these double-barred galaxies (Fathi et al. 2006). This is most notable in the case of NGC 5850.

In general, the gas distribution of our galaxies does not seem to be related to the main bars. This behaviour is unexpected, as ionised gas is commonly observed tracing the often present dust lanes seen along the main bar major axis (e.g., Athanassoula 1992; Patsis & Athanassoula 2000). Our result may be connected to the early-type nature of our galaxies (except for NGC 5850), which means that they do not have an appreciable dust content, as well as to the limited FoV sampled by our data. Unlike the case of the stellar kine-

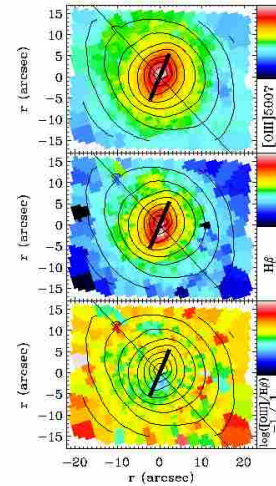


Figure 5. Gas intensity maps for NGC 5850. The top panel shows the intensity distribution of the $[\text{OIII}]\text{5007}$ emission line, whereas the middle panel corresponds to the $\text{H}\beta$ intensity. The distributions are different, with the $\text{H}\beta$ peak off-centred with respect to the stellar (shown with contours) and $[\text{OIII}]\text{5007}$ intensities. The corresponding kinematic maps (not shown here) are however equivalent, within the resolution of our data. The bottom panel shows the $[\text{OIII}]/\text{H}\beta$ ratio, which seems to indicate the presence of a small star-forming region at the position of the maximum $\text{H}\beta$ emission. For reference, the straight lines indicate the position and size of the inner (thick line) and outer (thin line) bars.

matics, the gas velocity dispersion maps are quite flat and show no signatures of the presence of the inner or the outer bars (see Appendix A).

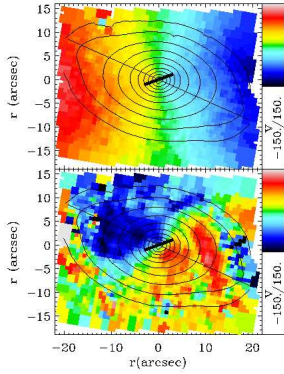


Figure 6. Stellar (top panel) and gas (bottom panel) velocity maps for NGC 3941, in km s^{-1} . The gas in NGC 3941 is clearly counter-rotating with respect to the stars. For reference, we have overplotted the position angle of the inner (thick line) and outer bar (thin line), and the contours of the reconstructed total intensity map.

5.2.2 $H\beta$ vs. $[OIII]5007$ gas distributions in NGC 5850

NGC 5850 is the only galaxy for which the gas distributions derived from the $[OIII]5007$ and $H\beta$ emission lines are different. The corresponding maps are shown in Figure 5. Whereas the $[OIII]5007$ distribution matches well with the stellar intensity distribution, the $H\beta$ map shows the maximum off-centred with respect to the stellar isophotes. However, this remarkable difference is not translated into kinematical differences, at least within the resolution of our data, since the gas velocity and velocity dispersion maps obtained from the two emission lines seem equivalent.

The position of the $H\beta$ emission peak in NGC 5850 corresponds with a small potential star-forming region, as indicated by the $[OIII]/H\beta$ ratio map also shown in Figure 5. This result is confirmed by Bremer et al. (2012) in a study of optical diagnostic diagrams using VIMOS integral-field spectroscopy. In addition they found a faint, second star-forming region 1.6 kpc (i.e., ~ 11.4 arcsec) East of the centre, which is not observed in our data. Their study favours the LINER nature of the nucleus. Note also that none of these potential star-forming regions is spatially coincident with the CO peak mentioned in Section 2 (Leon et al. 2000), which is located to the North of the centre. Unfortunately our data do not allow us to determine the extent to which the star-forming region(s) are due to the inner bar.

5.2.3 Counter-rotating gas in NGC 3941

Figure 6 compares the velocity fields corresponding to the stars and gas in NGC 3941, showing that the components are clearly decoupled and almost counter-rotating. Counter-rotation is not a peculiar feature, as Bertola et al. (1992) estimated that 10% to 20% of S0 galaxies have such a gas component. Subsequent studies have found even higher values ($\gtrsim 20\%$) for this fraction (e.g., Pizzella et al. 2004; Bureau & Chung 2006, among others). These results contrast with the markedly different incidence of counter-rotation in stellar components ($\sim 10\%$ in S0s, see Kuijken et al. 1996; Emsellem et al. 2011). It is therefore worth noting cases where gaseous and

stellar counter-rotating discs are present (see the case of NGC 5719 in Coccato et al. 2011).

The counter-rotation in NGC 3941 was already noticed by Fisher (1997), who suggests that it is probably the result of a merger event or accretion of gas with opposite angular momentum between them. In fact, merging is one of the most popular explanations for the presence of these kinds of structures (Ciri et al. 1995; Barnes 2002), even in the case of stellar discs (Eliche-Moral et al. 2011). There are however other possibilities, such as the appearance of *anomalous orbits* within a triaxial and tumbling potential, such as that of a bar (Emsellem & Arsenault 1997; Falcón-Barroso et al. 2004). These anomalous orbits are a family of close, stable, retrograde orbits, which are tilted with respect to the equatorial plane. Therefore, they can capture the ionised gas, thus forming the counter-rotating disc. Given that the kinematical major axis of the gas in NGC 3941 seems to be aligned with the main bar and that this galaxy is isolated, anomalous orbits seem to be the most likely explanation for the counter-rotating gas disc in NGC 3941.

6 STELLAR POPULATIONS

6.1 Line-strength maps

In order to investigate which stellar populations are shaping the double-barred galaxies, we measured the most relevant absorption line-strength indices over the emission-cleaned spectra covering the full SAURON FoV. The first necessary step, for the proper comparison of all Voronoi bins and galaxies, was the homogenisation (i.e., degradation) of all spectra to the same total broadening. We chose to degrade our data to a total full-width half maximum of 8.4 \AA to match the LIS- 8.4 \AA system proposed by Vazdekis et al. (2010). This new LIS system introduces several advantages with respect to the traditional Lick/IDS spectral system (Worthey et al. 1994): it avoids the lack of flux-calibration and the well-known wavelength dependence of the resolution (Worthey & Ottaviani 1997).

We calculated the age-sensitive $H\beta$ and the metallicity-sensitive Mgb and $Fe5015$ indices, following the Lick definitions given by Trager et al. (1998). Total metallicity is estimated from the $[MgFe50]'$ index, defined by Kuntschner et al. (2010). $[MgFe50]'$ has been proved to be a good metallicity indicator, almost insensitive to the $[Mg/Fe]$ overabundance. This index is mostly used by users of the SAURON spectrograph (see for example Ganda et al. 2007), since it does not require the measurements of the $Fe5270$ and $Fe5335$ indices, necessary to compute the more common $[MgFe]'$ index (Thomas et al. 2003), which lie outside of the SAURON spectral range.

Figure 7 shows the $H\beta$ and $[MgFe50]'$ line-strength index distributions for the double-barred sample. These maps, together with those corresponding to the Mgb and $Fe5015$ indices, are included in Appendix A for each galaxy. It is remarkable that the total metallicity indicator $[MgFe50]'$ presents slightly higher values at the regions delimited by the inner bars. This fact suggests that inner bars are more metal-rich than their surroundings.

6.2 Quantifying the stellar population parameters

Double-barred galaxies are made of several components and, while a scenario in which the different structures are shaped by the redistribution of the existing stars formed in a single burst is possible,

$$^1 [MgFe50]' = \frac{0.69 \times Mgb + Fe5015}{2}$$

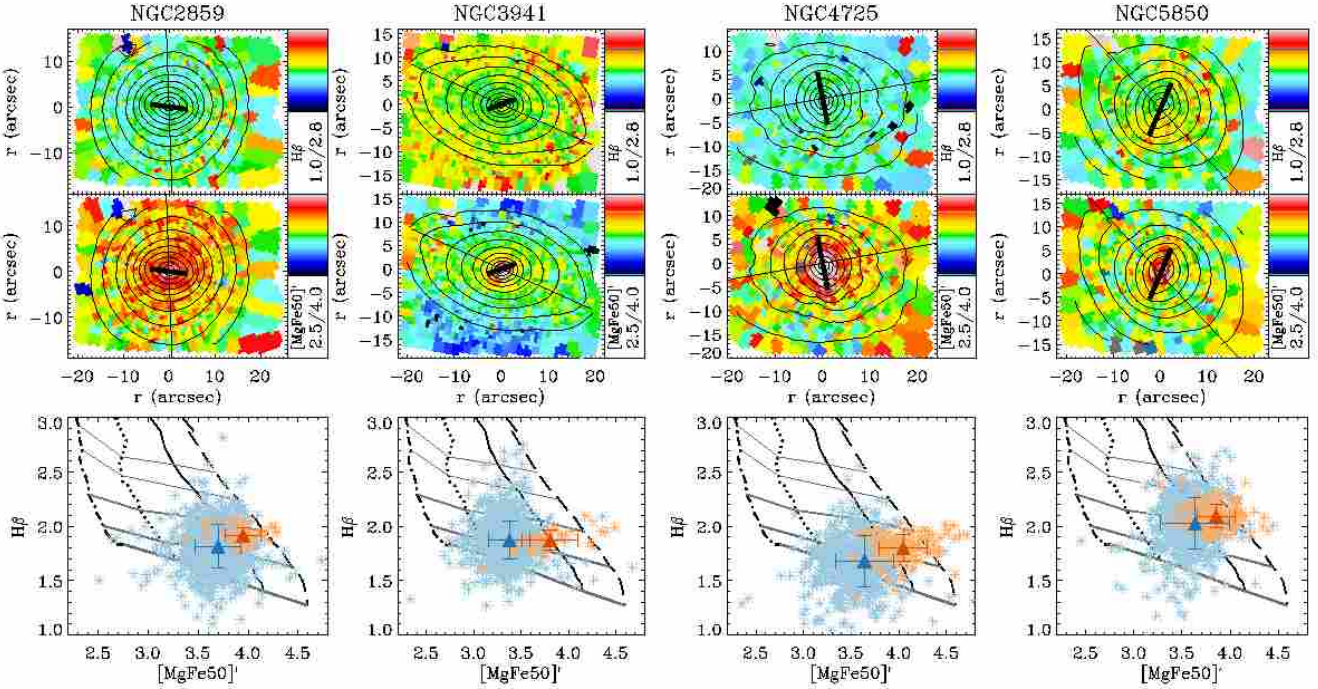


Figure 7. $H\beta$ (top panels) and $[MgFe50]'$ (middle panels) index distributions for NGC 2859, NGC 3941, NGC 4725, and NGC 5850 (from left to right). The slightly higher values of $[MgFe50]'$ present in the inner bar regions of the four double-barred galaxies suggest they are more metal-rich than their surroundings. The length and position angle of the inner and outer bars are indicated by thick and thin lines, respectively, and the contours of the reconstructed total intensity maps are also overplotted. The bottom row shows the $H\beta$ versus $[MgFe50]'$ measurements corresponding to the SSP models by Vazdekis et al. (2010). The solid lines represent different ages increasing from top to bottom (2.5, 3, 5.6, 10, and 18 Gyr, respectively), whereas the almost vertical lines indicate different metallicities increasing from left to right ($[Z/H] = -0.7, -0.4, 0.0$, and 0.2 , respectively). The asterisks are the measurements for all the Voronoi bins of each galaxy, distinguishing the bins corresponding to the inner bar (orange asterisks) from those corresponding to the outer bar (blue asterisks). The triangles represent the average measurements for the inner bar (red triangles), and the rest of the galaxy (blue triangles). The average values indicate that inner bars are coeval or slightly younger than their surroundings. Both models and galaxy measurements are carried out in the LIS-8.4 Å system.

each region most likely results from the superposition of several stellar populations. Assuming that our galaxies are well described by SSPs, it is possible to derive the luminosity-weighted age and metallicity of all bins by comparing the line-strength measurements with the corresponding predictions from the SSP models. As for the kinematics, in the stellar population analysis we use the stellar population models of Vazdekis et al. (2010). The spectral resolution of these models is 2.51 Å (FWHM), constant over the whole spectral range (Falcón-Barroso et al. 2011). In order to compare the model predictions to the data, the model spectra have also been smoothed to the LIS-8.4 Å system. Figure 7 (bottom row) shows the results for the $H\beta$ versus $[MgFe50]'$ indices. The grids are not perfectly orthogonal due to the age-metallicity degeneracy. For simplicity, we distinguish between the regions dominated by the inner bar and its surroundings, i.e., mostly the outer bar. Similar plots for the rest of the metallicity-sensitive indices can be seen in Appendix B.

Since double-barred galaxies are structurally complex and the two-dimensional information is crucial, we created age and metallicity maps to investigate the distribution of the stellar populations. For this purpose, we adapted the r_{model}^2 code (Cardiel et al. 2003), specifically developed for this kind of stellar population analysis, to perform a bivariate interpolation of the $H\beta$ versus $[MgFe50]'$ grids. The resulting luminosity-weighted age and metallicity maps are shown in Figure 8. Interestingly, as seen in the bottom panels of

Figure 7, the four inner bars appear not only more metal-rich, but also slightly younger, than their surroundings.

$[Mg/Fe]$, $[CN/Fe]$, and other similar abundance ratios are fundamental parameters in a stellar population analysis, as they act as chemical clocks and allow us to infer the formation timescales of the bulk of the stellar population. In an analogous way to the $[MgFe50]'$ index, it is possible to derive the Mgb and $Fe5015$ metallicity distributions from the interpolation of the corresponding $H\beta$ versus Mgb and $H\beta$ versus $Fe5015$ model grids. The $[Z_{Mgb}/Z_{Fe5015}]$ ratio distribution can be then obtained in a heuristic way by subtracting the two metallicity maps. $[Z_{Mgb}/Z_{Fe5015}]$ can be considered a proxy of the $[Mg/Fe]$ overabundance, as a linear relation between the two ratios is expected (Peletier et al. 2007; Vazdekis et al. 2010); note however that the absolute values of the $[Z_{Mg}/Z_{Fe}]$ measurements are not the same as those used by other authors, who usually take combined Fe-indices, such as $Fe3^3$ (e.g., Thomas et al. 2011; de la Rosa et al. 2011). It is for that reason, and in order to avoid confusion with values in the literature, that we refer to our $[Mg/Fe]$ estimate as $[Z_{Mg}/Z_{Fe}]$.

Given the small dynamical range of the $[Mg/Fe]$ parameter, which typically acquires values between 0.0 (i.e., solar abundance) and 0.4, these kinds of maps are naturally noisier than the age or metallicity maps. The final $[Z_{Mg}/Z_{Fe}]$ overabundance distributions for the four double-barred galaxies are shown in Figure 8. They

² www.ucm.es/info/Astrof/software/rmodel/rmodel.html

³ $Fe3 = \frac{Fe4383 + Fe5270 + Fe5335}{3}$.

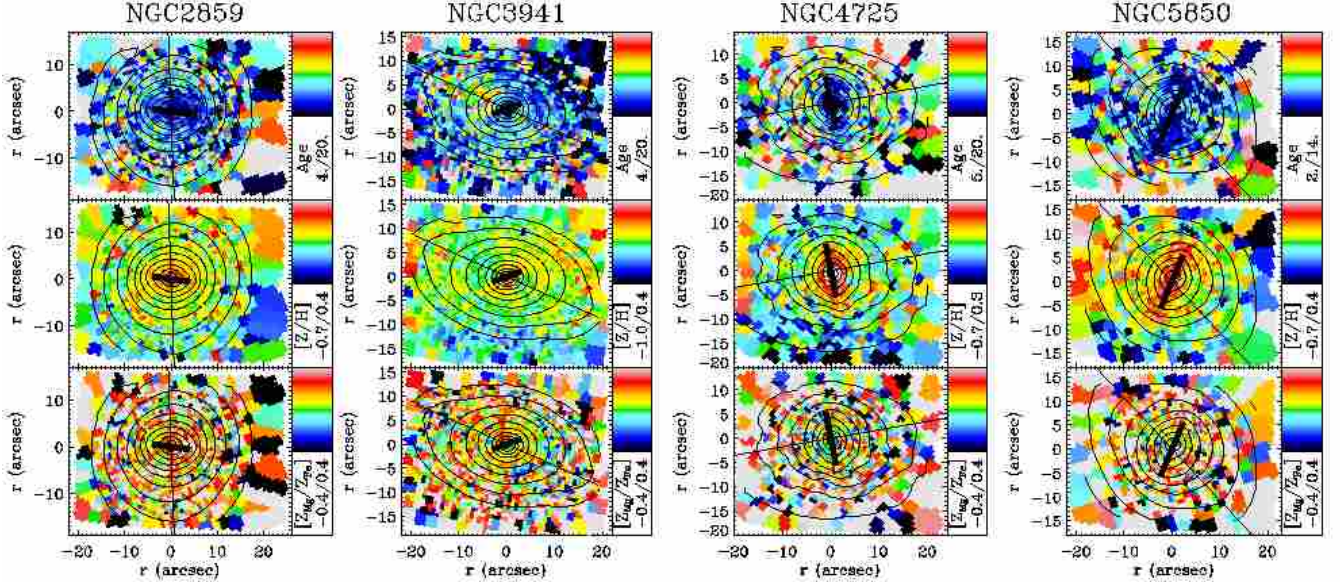


Figure 8. Luminosity-weighted age (in Gyr; top panels), metallicity ($[Z/H]$; middle panels), and $[Z_{\text{Mg}}/Z_{\text{Fe}}]$ (bottom panels) maps for NGC 2859, NGC 3941, NGC 4725, and NGC 5850 (from left to right, respectively). The maps are the result of interpolating the $H\beta$ versus $[MgFe50]'$ grids using the *rmodel* package. For the sake of clarity, we have overplotted the position angle and length of the inner (thick line) and outer (thin line) bars, and the contours of the reconstructed total intensity map. The inner bars appear clearly younger and more metal-rich than their surroundings, whereas the $[Z_{\text{Mg}}/Z_{\text{Fe}}]$ maps show rather flat distributions.

present flat distributions with typical values above 0. We therefore do not find significant differences between the inner and outer bar regions.

6.3 Radial profiles of the stellar population properties

In order to study in more detail the behaviour of the stellar population parameters from the inner to the outer regions in our data, we have also extracted radial profiles of the luminosity-weighted age, metallicity, and $[Z_{\text{Mg}}/Z_{\text{Fe}}]$. For this purpose we recover the PA, ellipticity, and semi-major axes of the best fitting ellipses to the flux maps calculated in Section 4, and run *KINEMETRY* again over the age, metallicity, and $[Z_{\text{Mg}}/Z_{\text{Fe}}]$ maps of Figure 8 to get the mean values of those parameters over the isophotes. Figure 9 shows that three out of the four double-barred galaxies present positive age gradients and negative metallicity gradients going outwards. The exception to this behaviour is illustrated by NGC 3941, which shows flat gradients in age, metallicity and abundance ratio in the regions dominated by the main bar.

Pérez et al. (2009) obtained the mean age and metallicity gradients along the main bars for a sample of 20 barred galaxies, eight of which are double-barred systems with one (NGC 2859) in common with our present sample. They found that main bars show both positive and negative age and metallicity gradients with no correlation between the two parameters, although there is a trend so that bars with negative metallicity gradients usually show positive age gradients, as in the general case of the galaxies presented here. Even among the double-barred galaxies of the Pérez et al. (2009) sample there are no clear correlations, with 50% of their double-bars showing positive age gradients, and also 50% positive metallicity gradients.

The variety of behaviours obtained by Pérez et al. (2009) is in contrast with the homogeneous trend found for our sample. However, Pérez et al. (2009) find that negative metallicity gradients tend

to appear in galaxies with the lowest central stellar velocity dispersions, with $\sigma < 170 \text{ km s}^{-1}$. Given that our four double-barred galaxies have maximum central velocity dispersion values ranging between 140 and 170 km s^{-1} , our results are actually in agreement with those of Pérez et al. (2009). Moreover, the radial profiles shown by Pérez et al. (2009) for NGC 2859 are fully consistent with those of Figure 9.

The $[Z_{\text{Mg}}/Z_{\text{Fe}}]$ radial profiles are rather flat with values ranging between 0.0 (i.e., solar abundance) and 0.3 dex, also in agreement with the results of Pérez et al. (2009). All the galaxies show a slight trend towards a positive gradient, so the central regions present lower values of the $[Z_{\text{Mg}}/Z_{\text{Fe}}]$ overabundance. This feature is almost unnoticed in the $[Z_{\text{Mg}}/Z_{\text{Fe}}]$ maps, which stresses the importance of analysing the data in different ways. The implications of this finding will be discussed in Section 7.

6.4 The characteristic stellar population properties of each structural component

Our last approach to analyse the stellar population content of the double-barred galaxies is to obtain the mean luminosity-weighted age, metallicity, and $[Z_{\text{Mg}}/Z_{\text{Fe}}]$ values in three regions of interest: a central region defined as a circle of radius 1 arcsec; the inner bar, defined as an ellipse with the corresponding PA, ellipticity, and semi-major axis characteristic of each inner bar (as given in Table 1), after subtracting the central 1 arcsec-circle; and the outer bar region, which is defined as an ellipse with the PA and ellipticity of the corresponding outer bar as given in Table 1 and a semi-major axis that is 5 arcsec longer than the semi-major axis length of the inner bar. With this criterion we assure that the considered outer bar region is inside the SAURON FoV and we avoid the very outer bins that present lower S/N . The central bins corresponding to the inner bar region are also removed from the outer bar definition in order to

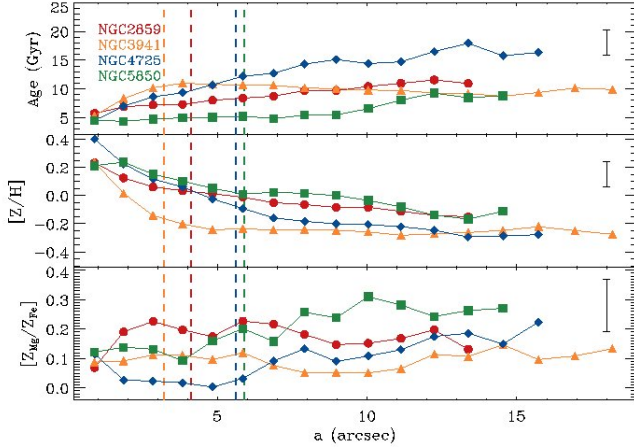


Figure 9. Mean luminosity-weighted age (top panel), metallicity (middle panel), and $[Z_{\text{Mg}}/Z_{\text{Fe}}]$ (bottom panel) profiles measured over the best fitting ellipses of the corresponding intensity map (see text for details). The x-axis represents the semi-major axes of the ellipses. Different colours and symbols correspond to different galaxies: NGC 2859 (red circles); NGC 3941 (yellow triangles), NGC 4725 (blue diamonds), and NGC 5850 (green squares). Vertical dashed lines indicate the length of the inner bars, as given in Table 1, whereas the mean error is indicated at the top right of each panel. The positive and negative gradients outwards in age and metallicity, respectively, are evident, whereas the $[Z_{\text{Mg}}/Z_{\text{Fe}}]$ profile shows a slight trend towards lower values at the central regions.

avoid the mixing of components. We deliberately ignore the bulge as it is not straightforward to delimit its extent from our data.

Figure 10 shows the mean values of the parameters in the bins inside each region of interest, with the corresponding dispersion represented by the error bars. Note that, as expected, the general trends shown in Section 6.3 appear also among structural components, namely the inner structures are always younger and more metal-rich than the outer ones, as seen in the age and metallicity maps of Figure 8.

de Lorenzo-Cáceres et al. (2012) studied the stellar populations of the bulge, inner bar, and outer bar of the double-barred early-type galaxy NGC 357. They found that inner structures, i.e., bulge and inner bar, showed approximately the same mean luminosity-weighted age (~ 8 Gyr) and solar metallicity, whereas the outer bar had a similar age and clearly lower metallicity. Taking into account that de Lorenzo-Cáceres et al. (2012) integrated the whole bulge region and not only the very central part, the results obtained for NGC 357 are compatible with the general conclusions derived for the present sample. In fact, the negative metallicity gradient exists in the five double-barred galaxies. Moreover, the five inner bars show approximately solar metallicity values and ages around ~ 7 Gyr.

The $[Z_{\text{Mg}}/Z_{\text{Fe}}]$ ratios for the central, inner bar, and outer bar regions also show the previously observed trend towards lower values in the central structures. Note that the four galaxies have a central abundance ratio around solar value, with $[Z_{\text{Mg}}/Z_{\text{Fe}}] \sim 0.05$ dex. It is known that ellipticals tend to have enhanced abundance ratios (e.g., Worthey et al. 1992), and bulges of many early-type spirals usually mimic the α -enhancement of ellipticals with a similar velocity dispersion (e.g., Jørgensen 1999; Kuntschner 2000; Vazdekis et al. 2004; Carretero et al. 2004). Following this relation, early-type spirals of central stellar velocity dispersions of $140\text{--}180 \text{ km s}^{-1}$ should have $[Mg/Fe] \sim 0.2\text{--}0.4$ dex, well above the central values

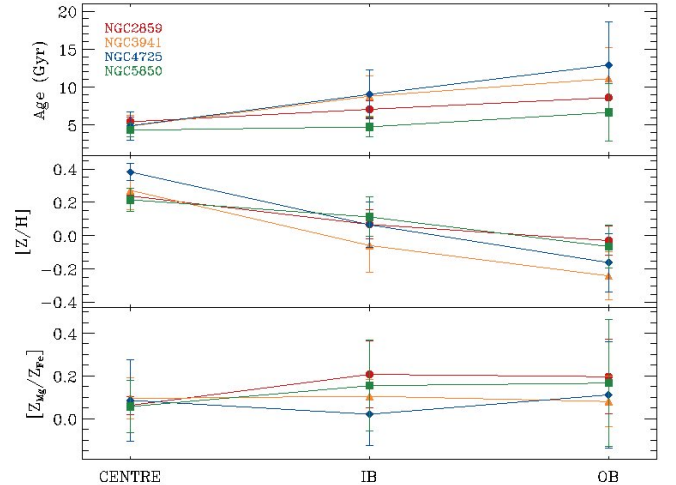


Figure 10. Mean luminosity-weighted age (top panel), metallicity (middle panel), and $[Z_{\text{Mg}}/Z_{\text{Fe}}]$ (bottom panel) values for the regions corresponding to a central circle with a 1 arcsec radius (CENTRE), inner bar (IB), and outer bar (OB; see text for details on the OB definition). Different colours and symbols correspond to different galaxies: NGC 2859 (red circles), NGC 3941 (yellow triangles), NGC 4725 (blue diamonds), and NGC 5850 (green squares). The error bars indicate the dispersion of the values inside each region. The positive and negative gradients outwards in age and metallicity, respectively, are evident. The $[Z_{\text{Mg}}/Z_{\text{Fe}}]$ distribution shows a slight trend towards lower values at the centre.

found for our double-barred sample and closer to the mean abundance ratios of the bars. The low values presented here are nonetheless not unexpected if some recent star formation has taken place in the inner regions of the galaxies (e.g., Thomas & Davies 2006).

7 DISCUSSION

7.1 The formation and stability of double-barred systems

The formation of double-barred galaxies has been a matter of debate for more than two decades. Most of the work done to address this issue is based on numerical simulations that usually require the presence of a dissipative component, i.e., gas content, which is dynamically disturbed to form the inner bar. Friedli & Martinet (1993) tried to develop double-barred systems with numerical simulations including only a purely collisionless component. They concluded that the presence of the gas was needed to form the two bars. Once gas was included, they got different models in which the two bars formed simultaneously, or in which the inner bar was formed after (and thanks to) the main bar. These two bars rapidly decoupled from each other and rotated with different pattern speeds. This last result has been observationally confirmed (Corsini et al. 2003). Those initial simulations predicted, however, that the final systems were not long-lived since at least the inner bar would disappear $1\text{--}2$ Gyr after its formation.

Since 1993, many more studies have succeeded at simulating the formation (Heller et al. 2001; Shlosman & Heller 2002; Rautainen et al. 2002; Englmaier & Shlosman 2004; Heller et al. 2007) and also the dynamical evolution (e.g., Maciejewski & Sparke 2000; Maciejewski & Athanassoula 2007) of double-barred systems. These simulations have in common that they also need a fundamental dissipative component to create inner bars, mostly be-

cause gas flows along the outer bar and is captured by its x_2 orbits, subsequently decoupling and forming the inner bar. Within these scenarios, inner bars should be younger and probably more metal-rich than their surroundings.

The observational results presented in this work are compatible with the bulk of simulations that need dissipation to form the inner bars. The analysis of the emission lines reveals that the whole sample actually contains ionised gas and that this is probably flowing towards the central regions. Moreover, our inner bars have turned out to be slightly younger and more metal-rich than their surroundings (i.e., the outer bar). The gas-rich scenario is further supported by the ubiquitous presence of extended HI gas in all the galaxies of our sample.

In contrast to the simulations mentioned above, Debattista & Shen (2007) generated long-lived inner bars without the presence of any dissipative component, although they require the presence of a rapidly rotating structure at the centre of the galaxy that is created *ad hoc* in these simulations. Inner bars then formed through the redistribution of the already existing stars. Therefore, at the moment of bar formation there are no expected differences among the stellar populations of the inner bars and the surrounding components, unless some additional gas were present or accreted into the central regions. While such a burst might lead to a small age difference, it is not clear whether it could also reproduce the observed metallicity gradient.

Note that for our analysis we only use single stellar populations leading to mean luminosity-weighted ages, which are biased towards the most recent stellar components. We find a significant but not large difference between the derived ages for the inner and outer bars. It is important to be aware of the fact that in order to observationally disentangle the formation sequence of inner bars, not only the star formation history but also the dynamical evolution of the different structures need to be known. In fact, inner bars are dynamically distinguished structures and their formation might have a dynamical origin with no effect over their stellar populations. Recovering both the star formation history and dynamical evolution of a structurally complex system such as a double-barred galaxy is a very challenging goal.

Regarding the stability of bars, it is worth noting that our inner bars are not particularly young systems in absolute terms, since they have mean luminosity-weighted ages ranging from 4 to 8 Gyr. If the age of the stellar populations traces the age of the stellar inner bar structure, these intermediate-to-old mean luminosity-weighted values seem to indicate that inner bars are long-lived systems, in agreement with most of the simulations and with the high frequency of double-barred galaxies found in the Universe (Erwin & Sparke 2002; Laine et al. 2002). Disentangling the dynamical evolution of inner bars is again mandatory to take final conclusions on their stability.

7.2 The role of bars in galaxy evolution

Bars are non-axisymmetric components that redistribute the angular momentum of a galaxy, allowing the flow of material along them. It is therefore natural that inner bars are thought to be key systems in transporting gas to the very central regions, where they help to trigger star formation and contribute to the creation of spheroidal structures. Under this framework, double-barred galaxies would be outstanding systems from a secular evolution point of view, since they would promote the formation of bulges (e.g., Kormendy & Kennicutt 2004; Athanassoula 2005). Furthermore, it has been theoretically demonstrated that inner bars allow the material to get to the

innermost regions, where the gas flowing along a single bar is not able to reach. Within this scenario, inner bars might also contribute to the fueling of active galactic nuclei (hereafter AGNs; Shlosman et al. 1989, 1990).

In our analysis, we do not find differences between the galaxies hosting or not an AGN, so we are not able to shed light on the role of inner bars in fueling the AGNs. As indicated in Section 2, NGC 3941 and NGC 4725 are Seyfert 2 galaxies (Véron-Cetty & Véron 2006), NGC 5850 hosts a LINER (Bremer et al. 2012), and NGC 2859 shows no signs of nuclear activity. More double-barred galaxies are needed to do a proper statistical analysis and to draw conclusions on this matter.

The presence of ionised gas in the four observed double-barred galaxies and the rather young ages of the inner bars suggest that gas has actually reached the inner structures, more likely by flowing along outer bars, and triggered star formation there. These results therefore support the idea that secular evolution is taking place in the double-barred sample, at least at outer bar scales, and that it has had a major effect over the stellar population composition of inner bars.

Signatures of secular evolution also appear at inner bar scales, since we have also found possible evidence of gas flow through the inner bars towards the very central regions. It is therefore probable that some low-level star formation is taking place in these innermost regions. This hypothesis is also backed by the fact that the centres of our four double-barred galaxies present somewhat lower [Mg/Fe] values than the inner bars and outer regions, which points towards a progressive, time-extended formation. Notwithstanding, this star formation seems to be not efficient nor strong enough to be inducing major morphological changes in the four double-barred galaxies. If inner bars were playing a major role in the formation of new structures in the central regions, these new structures should show up in a stellar population analysis such as the one performed in this work.

8 SUMMARY AND CONCLUSIONS

We have performed a detailed analysis of the kinematics and stellar populations of a sample of four double-barred early-type galaxies (NGC 2859, NGC 3941, NGC 4725, and NGC 5850), paying special attention to the spatial distribution of the properties provided by the high-quality SAURON integral-field spectroscopic data.

The analysis of the stellar and gas kinematics reveals a wide variety of structures: three of the four galaxies show signatures of the presence of a kinematically-decoupled stellar inner disc, which supports the idea that most barred galaxies contain a disc-like central component (Pérez et al. 2009), although it is important to notice that none of our four double-barred galaxies present a σ -drop at their centres (Emsellem et al. 2001), despite the fact that these drops usually appear in barred galaxies.

The stellar σ -hollows (de Lorenzo-Cáceres et al. 2008) appear in the four galaxies exactly at the edges of the inner bars. These hollows are kinematical signatures of the presence of inner bars, produced by the contrast between the high stellar velocity dispersion of the bulge and the lower velocity dispersion of the bar.

Concerning the gas kinematics, we find possible evidence of gas inflow towards the central regions in both the gas intensity and velocity maps. One out of the four galaxies, NGC 3941, contains gas which is counter-rotating with respect to the stellar component, whereas NGC 5850 is the only galaxy which shows differences between the [OIII]5007 and H β gas distributions.

The main result of this work is the distinct stellar populations found for the inner bars of the four galaxies: they are clearly younger and more metal-rich than the outer bars. Moreover, we find positive age and negative metallicity gradients along the inner and outer bars for all the galaxies except NGC 3941, which only shows the gradients inside the inner bar region, whereas the profiles along the outer bars are flat. It is important to notice that NGC 3941 tends to stand out with respect to the other three galaxies in all the studies: its inner bar is the smallest and most difficult to appreciate in the photometrical analysis and in the maps, it does not contain an inner disc, its gas is counter-rotating, and its stellar population radial profiles present slight differences with respect to the others. Notwithstanding, the main conclusions of this work apply also to this galaxy.

We have also analysed the [Mg/Fe] abundance ratio for the four double-barred galaxies, finding rather flat overabundance distributions; however, the very central regions of the four galaxies present almost solar $[Z_{\text{Mg}}/Z_{\text{Fe}}]$ ratios, with values slightly below the mean overabundances of the inner and outer bars. This result indicates a long star formation process in the very central region of these galaxies.

Although some of the results obtained in this work seem to indicate that inner bars are contributing to star formation at the centres of the galaxies, the efficiency of this process is, at present, low and thus not important enough to promote major morphological changes. This conclusion is somewhat understandable for our double-barred galaxies, since they are mainly early-type objects, for which the secular processes are expected to play a moderate role in the morphological evolution.

ACKNOWLEDGMENTS

The authors are indebted to Isaac Shlosman, Reynier Peletier, John Beckman, Jairo Méndez-Abreu, and J. Alfonso L. Aguerri for many fruitful discussions and comments on the manuscript. The careful reading as well as the interesting comments from the anonymous referee have substantially improved the article. Support from the SAURON team has been essential during the observations and early stages of the data analysis. AdLC thanks the *barred galaxies-girls* (Patricia Sánchez-Blázquez, Isabel Pérez, and Inma Martínez-Valpuesta) for their sincere interest in this work, Agnieszka Rys for her advice about the writing, and Luis Peralta for his positive attitude. AdLC also acknowledges partial financial support from ESA/ESTEC and a European Union EARA Fellowship for visiting the Leiden Observatory. JFB is supported by a Ramón y Cajal fellowship of the Spanish Ministry of Economy and Competitiveness. This research has been funded by the Spanish Ministry of Economy and Competitiveness under the grants AYA2010-21322-C03-02 and AIB-2010-DE-00227, and is based on observations made with the William Herschel Telescope, operated on the island of La Palma by the Isaac Newton Group in the Spanish Observatorio del Roque de los Muchachos of the Instituto de Astrofísica de Canarias. The work has also made use of the NASA/IPAC Extragalactic Database (NED) which is operated by the Jet Propulsion Laboratory, California Institute of Technology, under contract with the National Aeronautics and Space Administration, and of the SDSS database. Funding for the SDSS and SDSS-II has been provided by the Alfred P. Sloan Foundation, the Participating Institutions, the National Science Foundation, the U.S. Department of Energy, the National Aeronautics and Space Administration, the Japanese

Monbukagakusho, the Max Planck Society, and the Higher Education Funding Council for England.

REFERENCES

- Aguerrri J. A. L., Méndez-Abreu J., Corsini E. M., 2009, *A&A*, 495, 491
- Athanassoula E., 1992, *MNRAS*, 259, 345
- Athanassoula E., 2005, *MNRAS*, 358, 1477
- Bacon R., Copin Y., Monnet G., Miller B. W., Allington-Smith J. R., et al. 2001, *MNRAS*, 326, 23
- Barnes J. E., 2002, *MNRAS*, 333, 481
- Bertola F., Buson L. M., Zeilinger W. W., 1992, *ApJ*, 401, L79
- Biegging J. H., Biermann P., 1977, *A&A*, 60, 361
- Bontempi P., Giroletti M., Panessa F., Orienti M., Doi A., 2012, *MNRAS*, 426, 588
- Bremer M., Scharwächter J., Eckart A., Zuther J., Fischer S., Valencia-S M., 2012, *Journal of Physics Conference Series*, 372, 012054
- Bureau M., Athanassoula E., 2005, *ApJ*, 626, 159
- Bureau M., Chung A., 2006, *MNRAS*, 366, 182
- Cameron E., Carollo C. M., Oesch P., Aller M. C., Bschorr T., et al. 2010, *MNRAS*, 409, 346
- Cappellari M., Copin Y., 2003, *MNRAS*, 342, 345
- Cappellari M., Emsellem E., 2004, *PASP*, 116, 138
- Cardiel N., Gorgas J., Sánchez-Blázquez P., Cenarro A. J., Pedraz S., et al. 2003, *A&A*, 409, 511
- Carretero C., Vazdekis A., Beckman J. E., Sánchez-Blázquez P., Gorgas J., 2004, *ApJ*, 609, L45
- Ciri R., Bettoni D., Galletta G., 1995, *Nature*, 375, 661
- Coccato L., Morelli L., Corsini E. M., Buson L., Pizzella A., et al. 2011, *MNRAS*, 412, L113
- Coelho P., Gadotti D. A., 2011, *ApJ*, 743, L13
- Comerón S., Knapen J. H., Beckman J. E., 2008, *A&A*, 485, 695
- Contopoulos G., Papayannopoulos T., 1980, *A&A*, 92, 33
- Corsini E. M., Debattista V. P., Aguerri J. A. L., 2003, *ApJ*, 599, L29
- de la Rosa I. G., La Barbera F., Ferreras I., de Carvalho R. R., 2011, *MNRAS*, 418, L74
- de Lorenzo-Cáceres A., Falcón-Barroso J., Vazdekis A., Martínez-Valpuesta I., 2008, *ApJ*, 684, L83
- de Lorenzo-Cáceres A., Vazdekis A., Aguerri J. A. L., Corsini E. M., Debattista V. P., 2012, *MNRAS*, p. 2170
- de Vaucouleurs G., de Vaucouleurs A., Corwin Jr. H. G., Buta R. J., Paturel G., Fouque P., 1991, *Third Reference Catalogue of Bright Galaxies*
- Debattista V. P., Shen J., 2007, *ApJ*, 654, L127
- Eliche-Moral M. C., González-García A. C., Balcels M., Aguerri J. A. L., Gallego J., et al. 2011, *A&A*, 533, A104
- Elmegreen B. G., Elmegreen D. M., Hirst A. C., 2004, *ApJ*, 612, 191
- Emsellem E., Arsenault R., 1997, *A&A*, 318, L39
- Emsellem E., Cappellari M., Krajnović D., Alatalo K., Blitz L., Bois M., Bournaud F., et al. 2011, *MNRAS*, 414, 888
- Emsellem E., Cappellari M., Peletier R. F., McDermid R. M., Bacon R., et al. 2004, *MNRAS*, 352, 721
- Emsellem E., Greusard D., Combes F., Friedli D., Leon S., et al. 2001, *A&A*, 368, 52
- Englmaier P., Shlosman I., 2004, *ApJ*, 617, L115
- Erwin P., 2004, *A&A*, 415, 941
- Erwin P., Sparke L. S., 2002, *AJ*, 124, 65

- Erwin P., Sparke L. S., 2003, *ApJS*, 146, 299
- Eskridge P. B., Frogel J. A., Pogge R. W., Quillen A. C., Davies R. L., DePoy D. L., Houdashelt M. L., Kuchinski L. E., Ramírez S. V., Sellgren K., Terndrup D. M., Tiede G. P., 2000, *AJ*, 119, 536
- Falcón-Barroso J., Bacon R., Bureau M., Cappellari M., Davies R. L., et al. 2006, *MNRAS*, 369, 529
- Falcón-Barroso J., Peletier R. F., Emsellem E., Kuntschner H., Fathi K., et al. 2004, *MNRAS*, 350, 35
- Falcón-Barroso J., Sánchez-Blázquez P., Vazdekis A., Ricciardelli E., Cardiel N., et al. 2011, *A&A*, 532, A95
- Fathi K., Storch-Bergmann T., Riffel R. A., Winge C., Axon D. J., Robinson A., Capetti A., Marconi A., 2006, *ApJ*, 641, L25
- Fisher D., 1997, *AJ*, 113, 950
- Friedli D., Martinet L., 1993, *A&A*, 277, 27
- Ganda K., Falcón-Barroso J., Peletier R. F., Cappellari M., Emsellem E., et al. 2006, *MNRAS*, 367, 46
- Ganda K., Peletier R. F., McDermid R. M., Falcón-Barroso J., de Zeeuw P. T., et al. 2007, *MNRAS*, 380, 506
- Gerhard O. E., 1993, *MNRAS*, 265, 213
- Heller C., Shlosman I., Englmaier P., 2001, *ApJ*, 553, 661
- Heller C. H., Shlosman I., Athanassoula E., 2007, *ApJ*, 657, L65
- Higdon J. L., Buta R. J., Purcell G. B., 1998, *AJ*, 115, 80
- Ho L. C., Filippenko A. V., Sargent W. L. W., 1997, *ApJ*, 487, 591
- Jablonka P., Gorgas J., Goudfroij P., 2007, *A&A*, 474, 763
- Jedrzejewski R. I., 1987, *MNRAS*, 226, 747
- Jogee S., Barazza F. D., Rix H. W., Shlosman I., Barden M., et al. 2004, *ApJ*, 615, L105
- Jørgensen I., 1999, *MNRAS*, 306, 607
- Kissler-Patig M., Copin Y., Ferruit P., Pécontal-Rousset A., Roth M. M., 2004, *Astronomische Nachrichten*, 325, 159
- Kormendy J., Kennicutt Jr. R. C., 2004, *ARA&A*, 42, 603
- Krajnović D., Cappellari M., de Zeeuw P. T., Copin Y., 2006, *MNRAS*, 366, 787
- Kuijken K., Fisher D., Merrifield M. R., 1996, *MNRAS*, 283, 543
- Kuntschner H., 2000, *MNRAS*, 315, 184
- Kuntschner H., Emsellem E., Bacon R., Cappellari M., Davies R. L., et al. 2010, *MNRAS*, 408, 97
- Laine S., Shlosman I., Knapen J. H., Peletier R. F., 2002, *ApJ*, 567, 97
- Leon S., Combes F., Friedli D., 2000, in Combes F., Mamon G. A., Charmandaris V., eds, *Dynamics of Galaxies: from the Early Universe to the Present Vol. 197 of Astronomical Society of the Pacific Conference Series, Single CO Peak in the Double Bar Galaxy NGC 5850*. p. 61
- Lisker T., Grebel E. K., Binggeli B., 2006, *AJ*, 132, 497
- MacArthur L. A., 2005, *ApJ*, 623, 795
- Maciejewski W., Athanassoula E., 2007, *MNRAS*, 380, 999
- Maciejewski W., Sparke L. S., 2000, *MNRAS*, 313, 745
- Marinova I., Jogee S., 2007, *ApJ*, 659, 1176
- Márquez I., Durret F., Masegosa J., Moles M., González Delgado R. M., et al. 2000, *A&A*, 360, 431
- Márquez I., Masegosa J., Durret F., González Delgado R. M., Moles M., et al. 2003, *A&A*, 409, 459
- Moiseev A. V., 2001, *Bull. Special Astrophys. Obs.*, 51, 140
- Moiseev A. V., Valdés J. R., Chavushyan V. H., 2004, *A&A*, 421, 433
- Moorthy B. K., Holtzman J. A., 2006, *MNRAS*, 371, 583
- Muñoz-Tuñón C., Caon N., Aguerri J. A. L., 2004, *AJ*, 127, 58
- Patsis P. A., Athanassoula E., 2000, *A&A*, 358, 45
- Peletier R. F., Falcón-Barroso J., Bacon R., Cappellari M., Davies R. L., et al. 2007, *MNRAS*, 379, 445
- Pérez I., Sánchez-Blázquez P., 2011, *A&A*, 529, A64
- Pérez I., Sánchez-Blázquez P., Zurita A., 2007, *A&A*, 465, L9
- Pérez I., Sánchez-Blázquez P., Zurita A., 2009, *A&A*, 495, 775
- Petitpas G. R., Wilson C. D., 2004, *ApJ*, 603, 495
- Pfenniger D., Norman C., 1990, *ApJ*, 363, 391
- Pizzella A., Corsini E. M., Vega-Beltrán J. C., Bertola F., 2004, *A&A*, 424, 447
- Rautiainen P., Salo H., Laurikainen E., 2002, *MNRAS*, 337, 1233
- Sánchez-Blázquez P., Ocvirk P., Gibson B. K., Pérez I., Peletier R. F., 2011, *MNRAS*, 415, 709
- Sarzi M., Falcón-Barroso J., Davies R. L., Bacon R., Bureau M., et al. 2006, *MNRAS*, 366, 1151
- Serra P., Oosterloo T., Morganti R., Alatalo K., Blitz L., et al. 2012, *MNRAS*, 422, 1835
- Sheth K., Elmegreen D. M., Elmegreen B. G., Capak P., Abraham R. G., et al. 2008, *ApJ*, 675, 1141
- Sheth K., Vogel S. N., Regan M. W., Thornley M. D., Teuben P. J., 2005, *ApJ*, 632, 217
- Shlosman I., Begelman M. C., Frank J., 1990, *Nature*, 345, 679
- Shlosman I., Frank J., Begelman M. C., 1989, *Nature*, 338, 45
- Shlosman I., Heller C. H., 2002, *ApJ*, 565, 921
- Thomas D., Davies R. L., 2006, *MNRAS*, 366, 510
- Thomas D., Maraston C., Bender R., 2003, *MNRAS*, 343, 279
- Thomas D., Maraston C., Johansson J., 2011, *MNRAS*, 412, 2183
- Trager S. C., Worthey G., Faber S. M., Burstein D., González J. J., 1998, *ApJS*, 116, 1
- Tully R. B., 1988, *Nearby galaxies catalog*
- van der Marel R. P., Franx M., 1993, *ApJ*, 407, 525
- Vazdekis A., Sánchez-Blázquez P., Falcón-Barroso J., Cenarro A. J., Beasley M. A., et al. 2010, *MNRAS*, 404, 1639
- Vazdekis A., Trujillo I., Yamada Y., 2004, *ApJ*, 601, L33
- Véron-Cetty M. P., Véron P., 2006, *A&A*, 455, 773
- Wardle M., Knapp G. R., 1986, *AJ*, 91, 23
- Wevers B. M. H. R., Appleton P. N., Davies R. D., Hart L., 1984, *A&A*, 140, 125
- Worthey G., Faber S. M., González J. J., 1992, *ApJ*, 398, 69
- Worthey G., Faber S. M., González J. J., Burstein D., 1994, *ApJS*, 94, 687
- Worthey G., Ottaviani D. L., 1997, *ApJS*, 111, 377
- York D. G., Adelman J., Anderson Jr. J. E., Anderson S. F., Annis J., et al. 2000, *AJ*, 120, 1579

APPENDIX A: ALL THE MAPS GALAXY BY GALAXY

In this Section we put together the maps resulting from the analysis of the SAURON data for each galaxy, including the stellar intensity and kinematics, gas intensity and kinematics, the measured line-strength indices, and the mean luminosity-weighted ages and metallicities.

APPENDIX B: INDEX-INDEX DIAGRAMS

The following Figures contain the results from the index-index diagram analysis: the model predictions for an age-sensitive index are plotted versus the predictions for a metallicity-sensitive index, and the same measurements for the data are overplotted in order to study the age and metallicity of our galaxies.

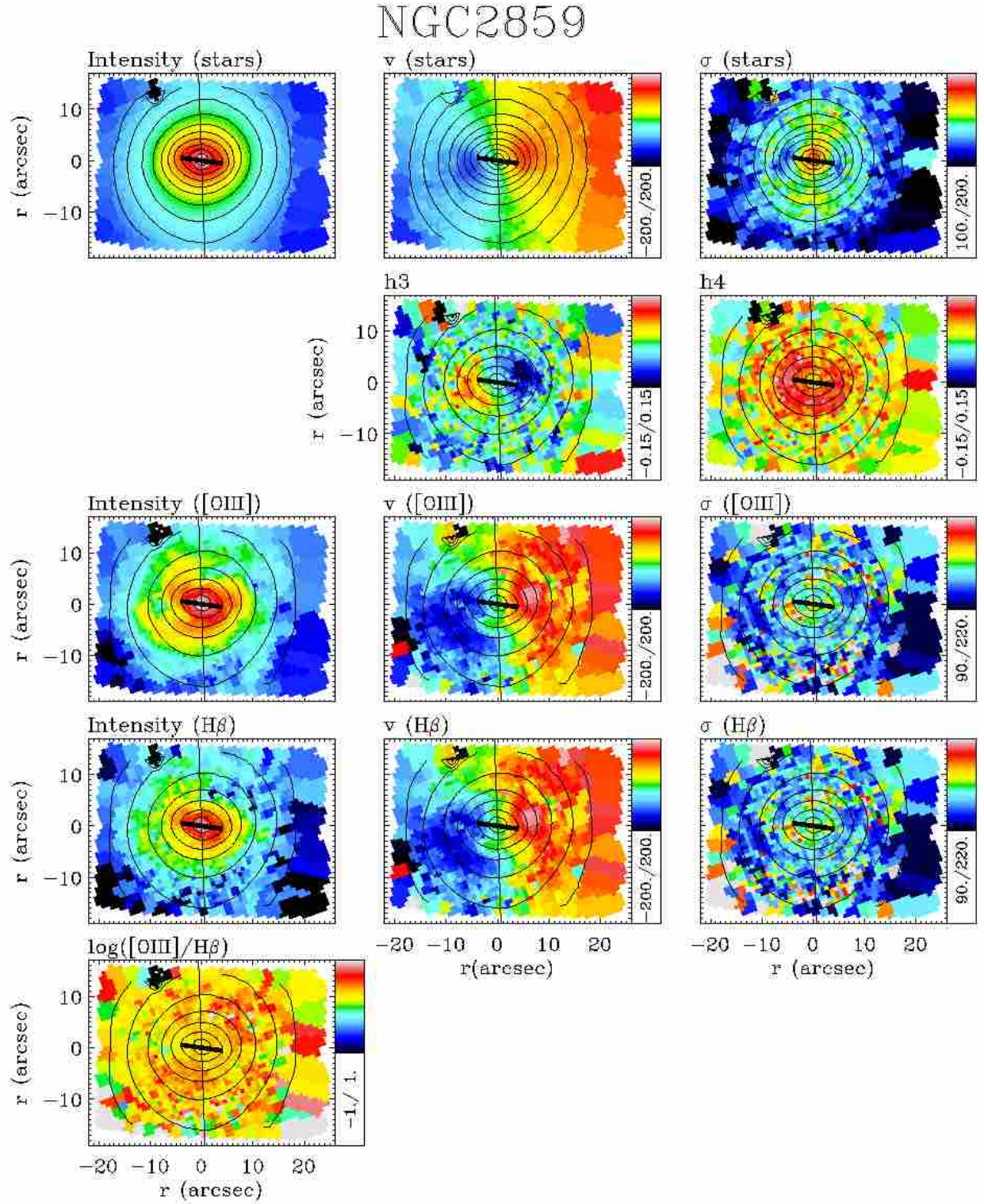


Figure A1. Kinematical analysis of the double-barred galaxy NGC 2859. The two top rows contain the stellar kinematics; from left to right and from top to bottom: stellar intensity (in arbitrary units), LOS velocity (km s^{-1}), velocity dispersion (km s^{-1}), h_3 , and h_4 maps. The third and fourth rows represent the gas kinematics derived from the [OIII] and $H\beta$ emission lines, respectively; from left to right: line intensity (arbitrary units), velocity (km s^{-1}), and velocity dispersion (km s^{-1}). The bottom panel is the [OIII]/ $H\beta$ gas intensity ratio in logarithmic scale. For all the maps, we have overplotted the position angle and length of the inner bar (thick line), the position angle of the outer bar (thin line), and the contours of the reconstructed total intensity map. The scale is 1 arcsec \sim 120 pc.

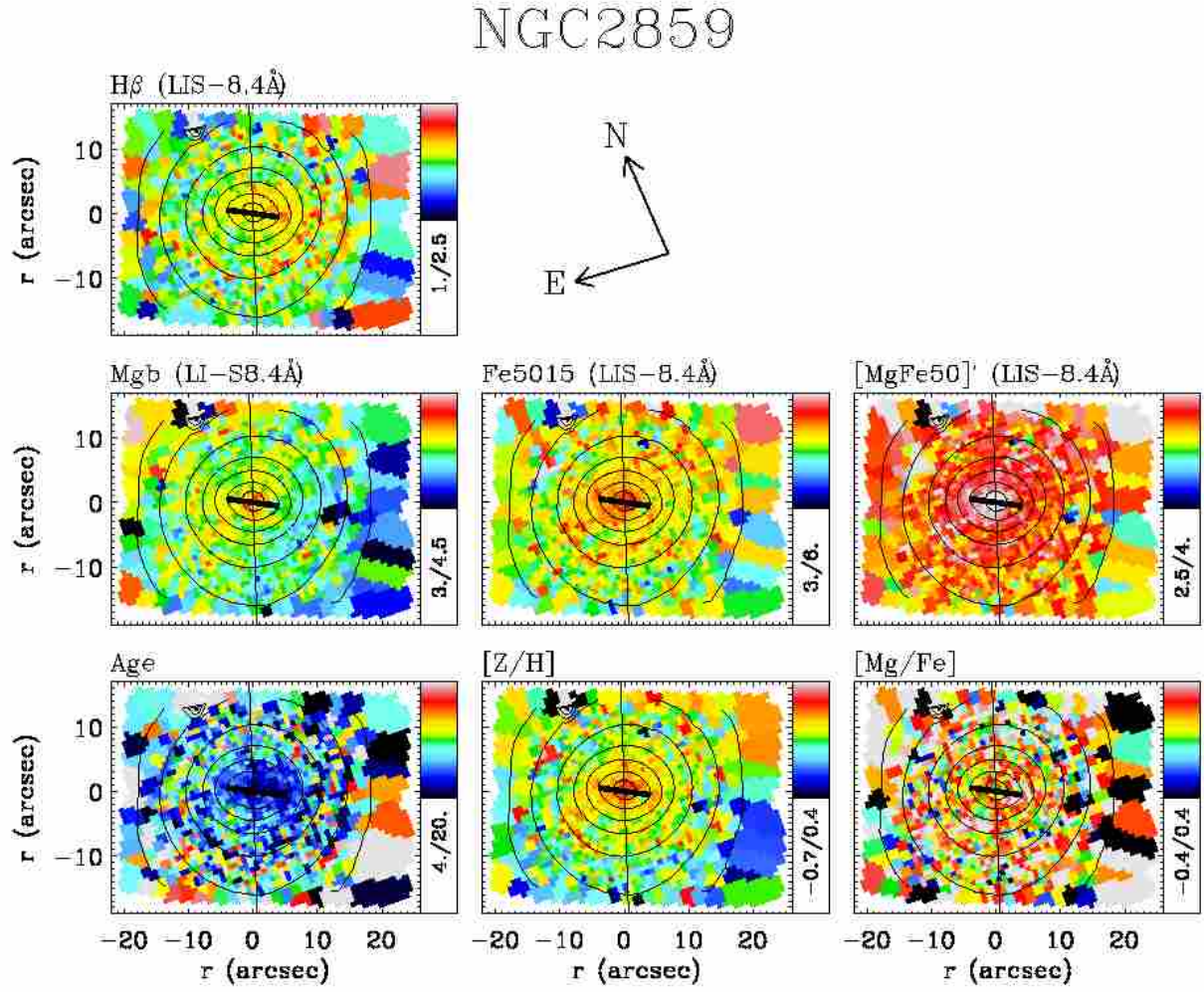


Figure A2. Stellar population analysis of the double-barred galaxy NGC 2859. The first row includes the map of the age-sensitive index $H\beta$, whereas the middle row shows the maps corresponding to the metallicity indicators Mgb , $Fe5015$, and $[MgFe50]'$ (from left to right, respectively). All the indices are measured at a resolution of 8.4 \AA (FWHM), following the corresponding LIS system. The bottom row contains the age (in Gyr), metallicity, and α -enhancement distributions, from left to right, respectively. For all the maps, we have overplotted the position angle and length of the inner bar (thick line), the position angle of the outer bar (thin line), and the contours of the reconstructed total intensity map. The relative orientation on the sky is also indicated. The scale is $1\text{ arcsec} \sim 120\text{ pc}$.

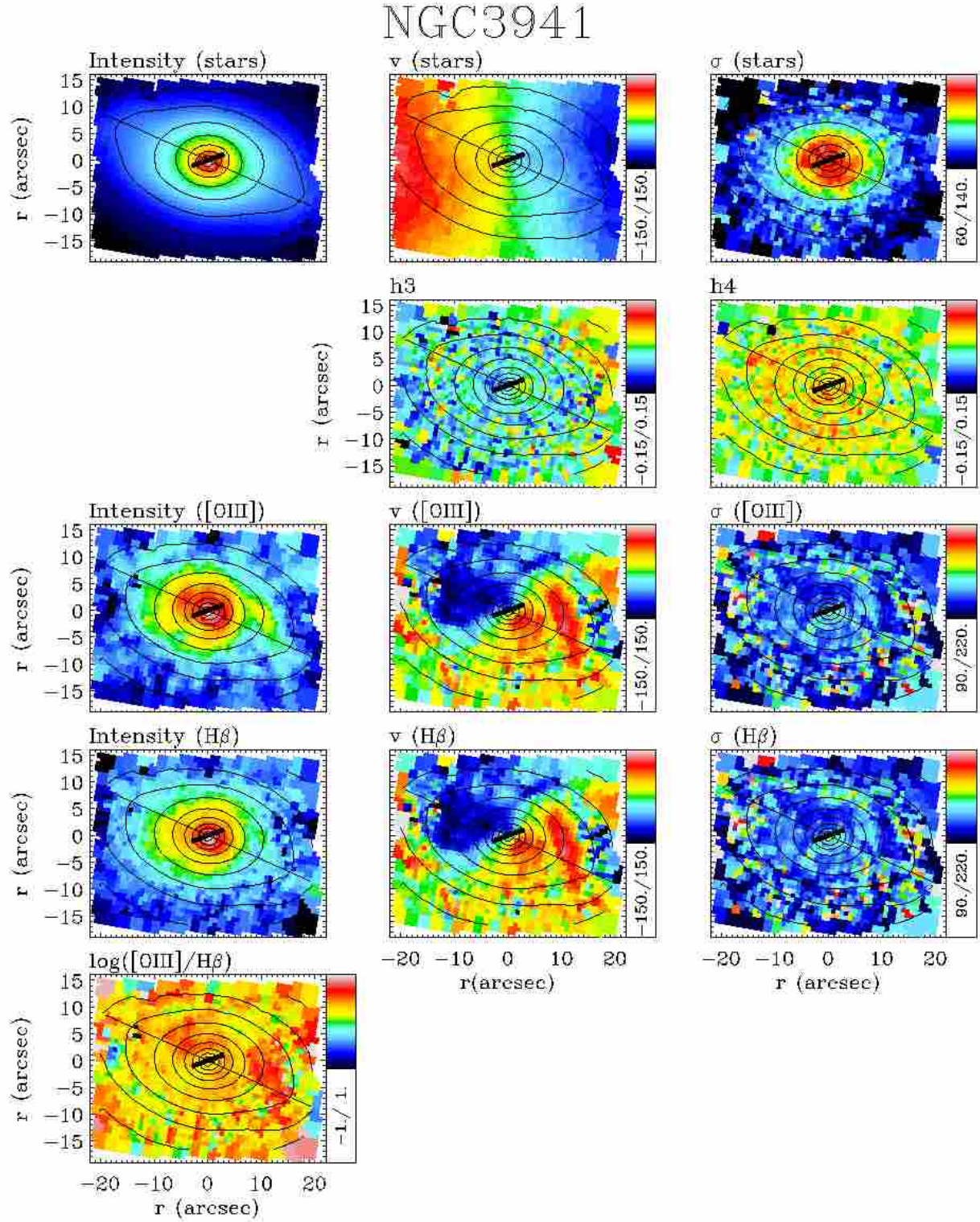


Figure A3. Same as Figure A1 but for NGC 3941. The scale is 1 arcsec \sim 90 pc.

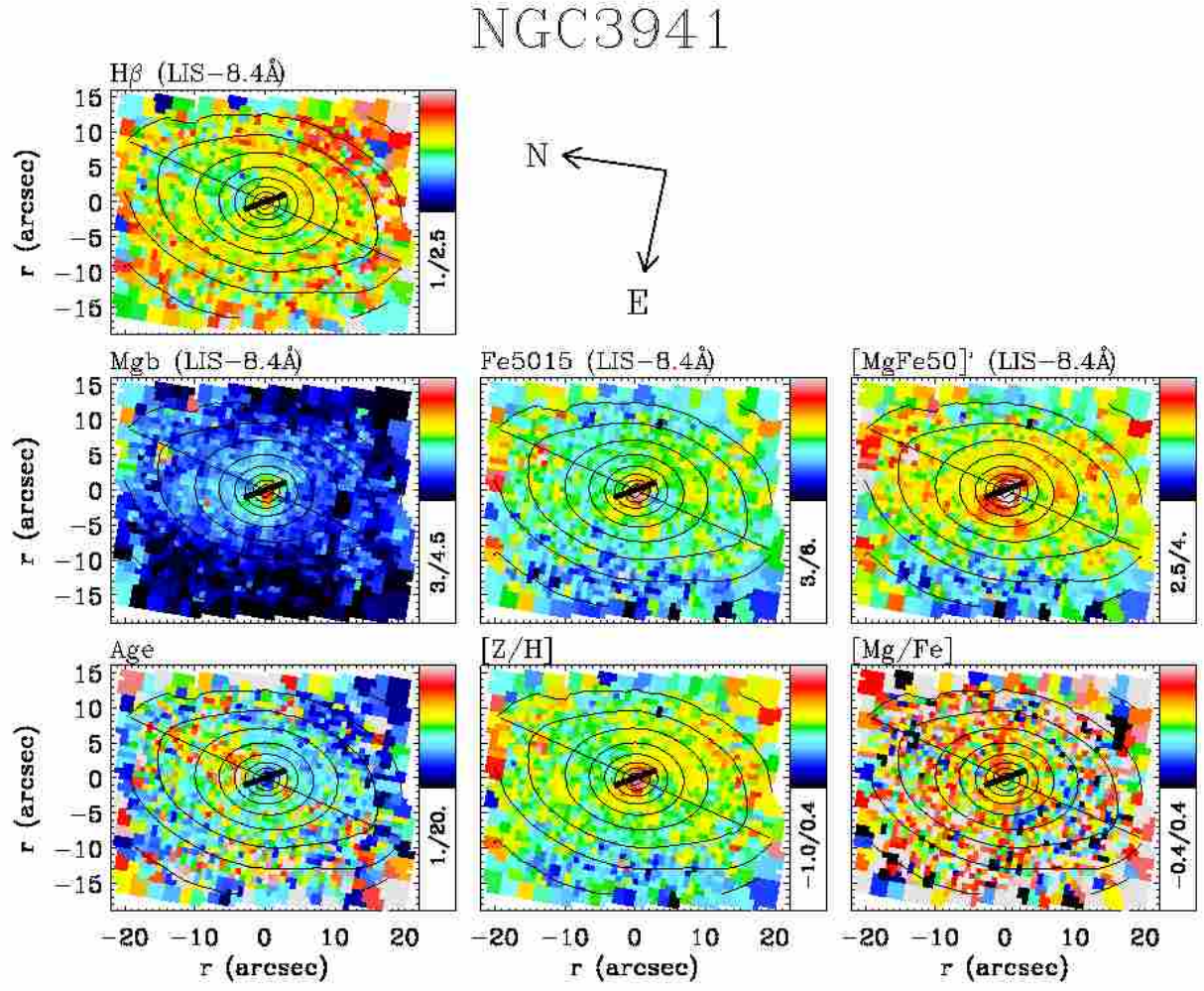


Figure A4. Same as Figure A2 but for NGC 3941. The scale is 1 arcsec \sim 90 pc.

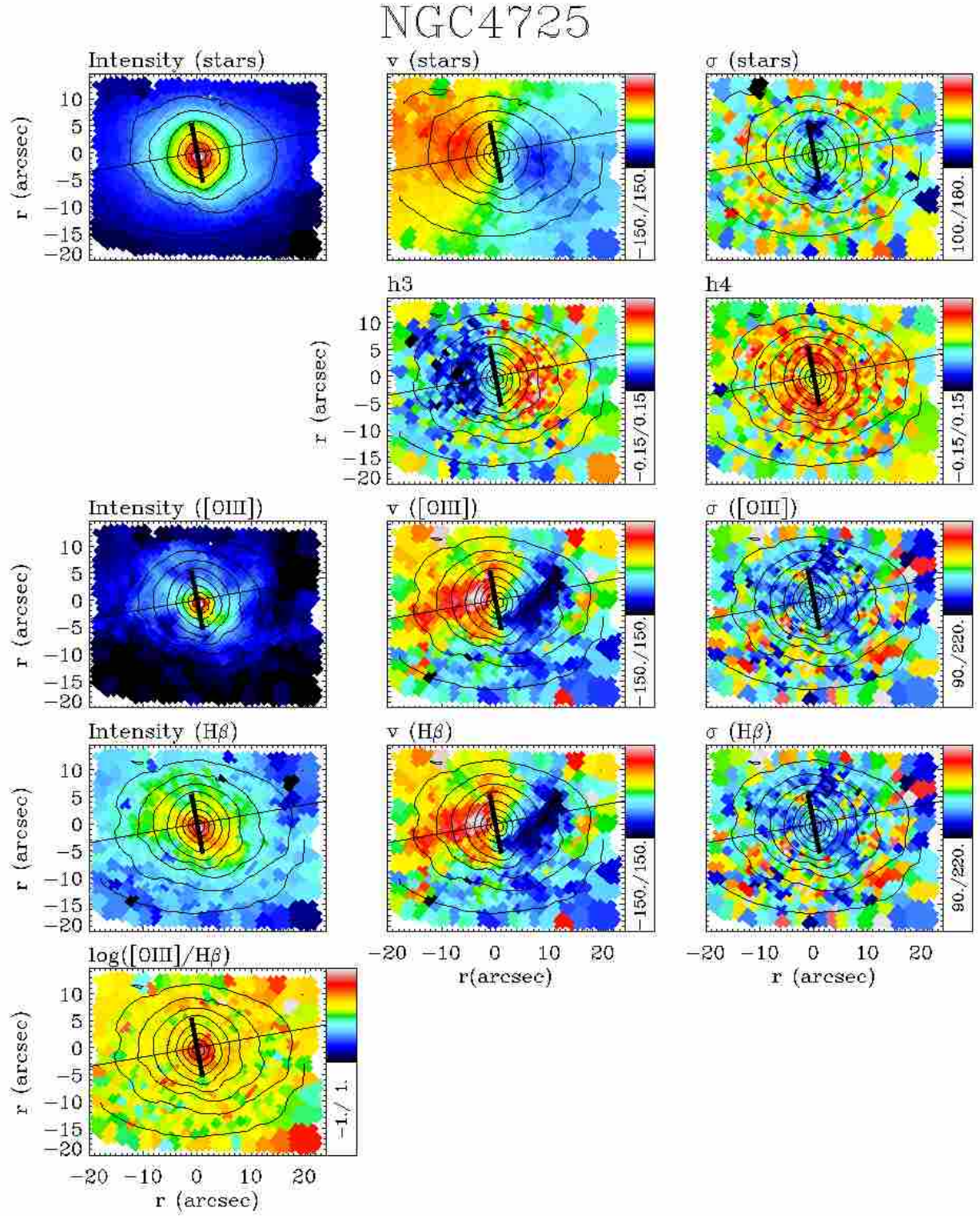


Figure A5. Same as Figure A1 but for NGC 4725. The scale is 1 arcsec \sim 60 pc.

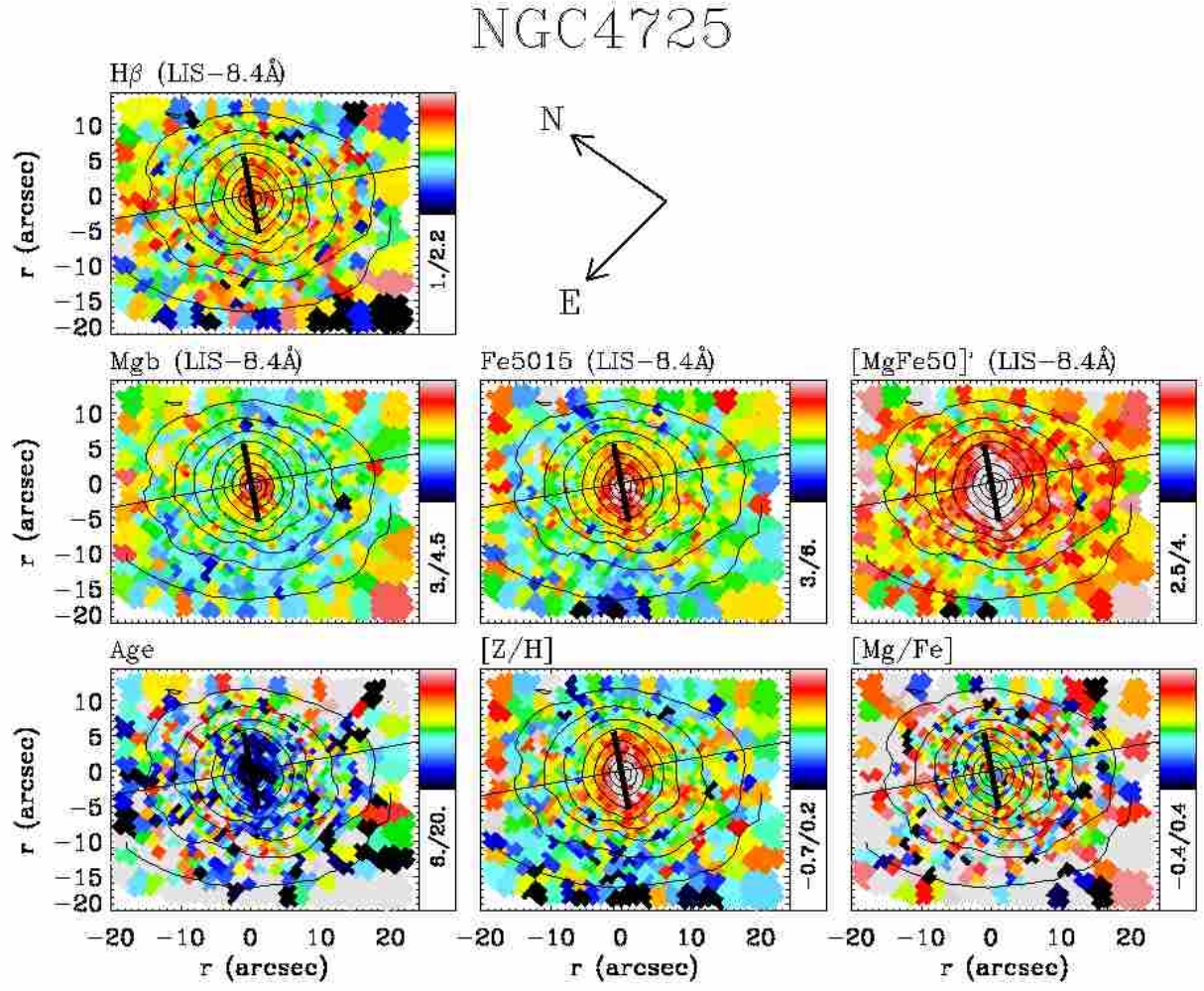


Figure A6. Same as Figure A2 but for NGC 4725. The scale is 1 arcsec \sim 60 pc.

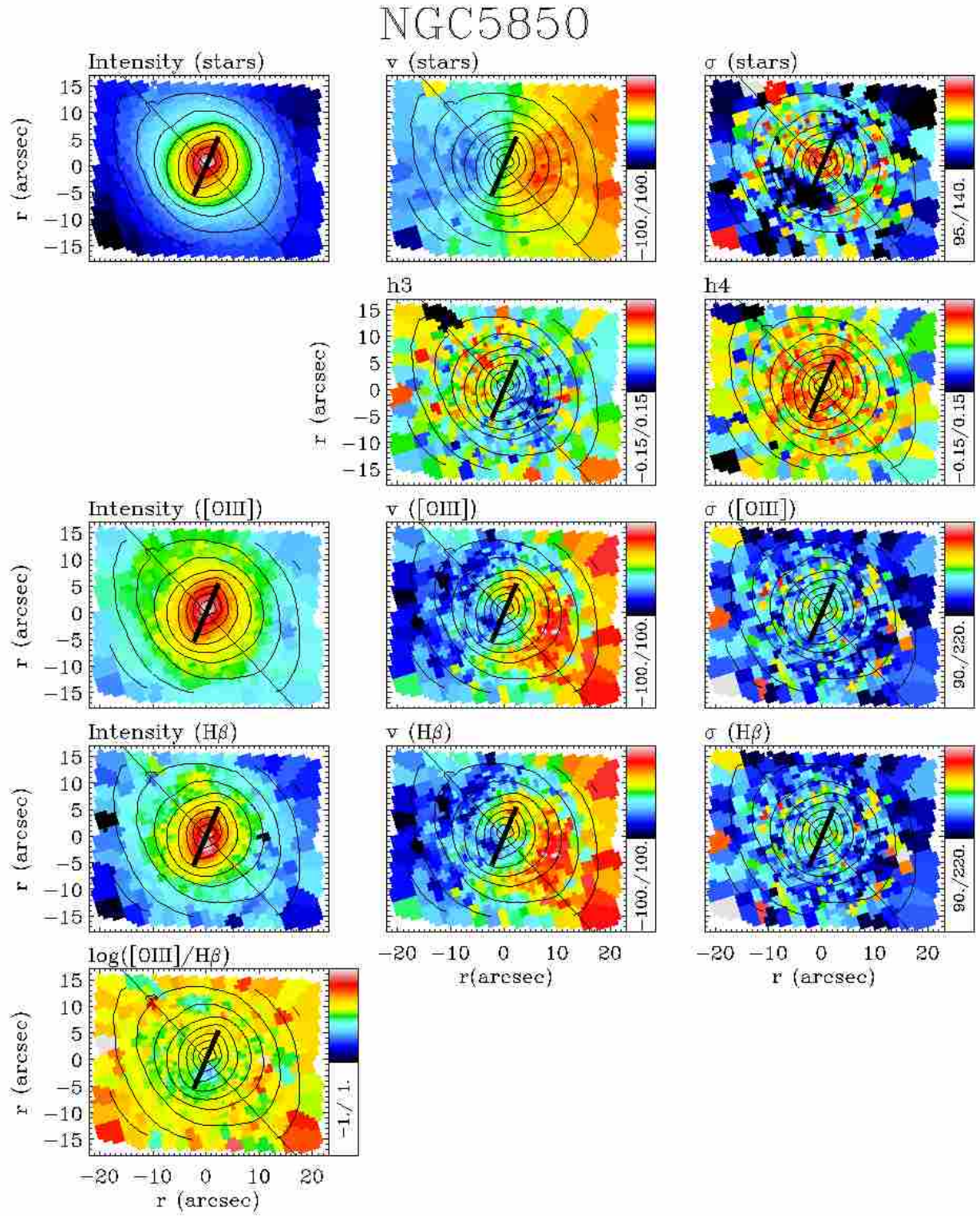


Figure A7. Same as Figure A1 but for NGC 5850. The scale is 1 arcsec \sim 140 pc.

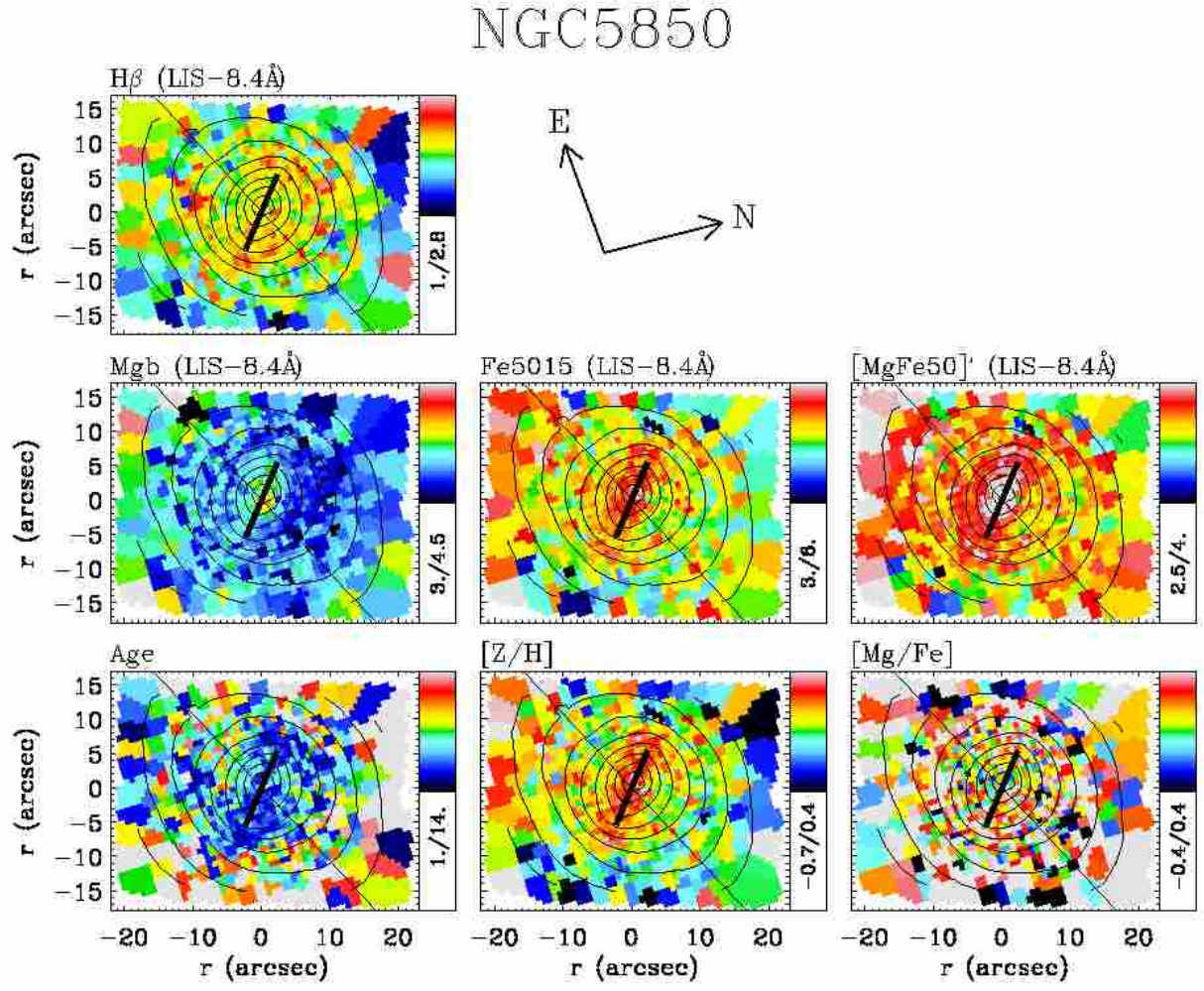


Figure A8. Same as Figure A2 but for NGC 5850. The scale is 1 arcsec \sim 140 pc.

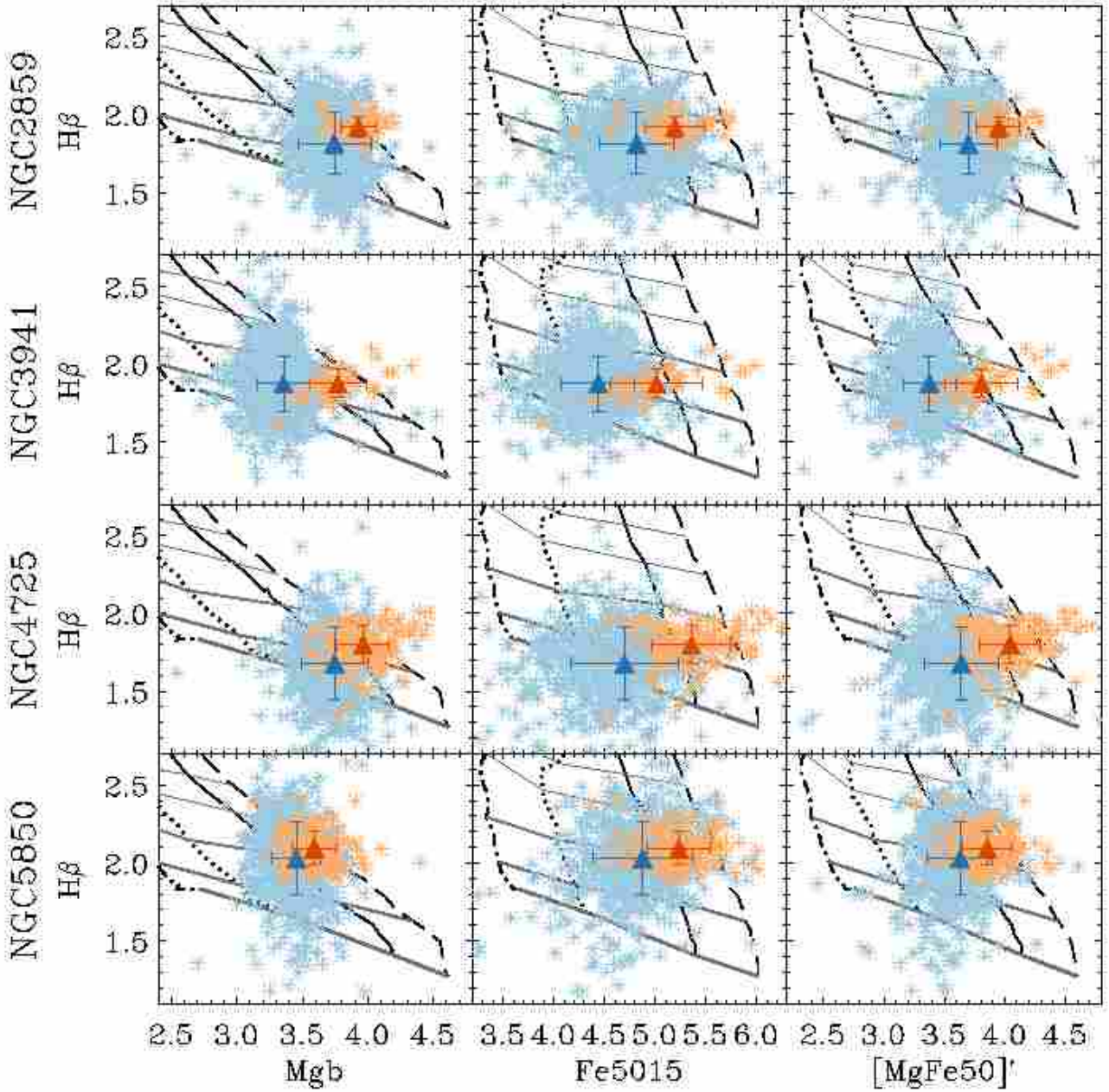


Figure B1. Age indicator $H\beta$ versus the metallicity indicators Mgb , $Fe5015$, and $[MgFe50]'$ (from left to right, respectively) for the four double-barred galaxies: NGC 2850, NGC 3941, NGC 4725, and NGC 5850 (from top to bottom, respectively). The grids correspond to the SSP models by Vazdekis et al. (2010). The solid lines represent different ages increasing from top to bottom (2.5, 3, 5.6, 10, and 18 Gyr, respectively), whereas the almost vertical lines indicate different metallicities increasing from left to right ($[Z/H] = -0.7, -0.4, 0.0$, and 0.2 , respectively). The asterisks are the measurements for all the Voronoi bins of each galaxy, distinguishing the bins corresponding to the inner bar (orange asterisks) from those corresponding to the outer bar (blue asterisks). The triangles represent the average measurements for the inner bar (red triangles), and the rest of the galaxy (blue triangles). Both models and galaxy measurements are carried out in the LIS-8.4 Å system.